JGR Atmospheres

RESEARCH ARTICLE
10.1029/2025JD044543

Special Collection:
Biomass Burning Uncertainties: Emissions, Chemistry, and Physics

Laboratory Experiments on Savannah and European Boreal Forest Fire Emissions

V. Vakkari[1,2], L. Vettikkat[3], S. Kommula[3], A. Mukherjee[3], L. Hao[3], J. Backman[1], A. Buchholz[3], N. Gawlitta[4,5], M. Ihalainen[6], K. Jaars[2], K. Köster[7], V. Le[1], P. Miettinen[6], A. Nissinen[3], H. Czech[4,8], M. Alton[3,9], J. Passig[8], S. Peltokorpi[3], A. A. Piedehierro[1], I. Pullinen[3], E. I. Rosewig[8], S. Schobesberger[3], D. Shukla[4,8], S. J. Siebert[10], M. Somero[6], A. Virkkula[1], A. Welti[1], P. Yli-Pirilä[6], A. Ylisirniö[3], R. Zimmermann[4,8], P. G. van Zyl[2], A. Virtanen[3], and O. Sippula[6,11]

[1]Finnish Meteorological Institute, Helsinki, Finland, [2]Atmospheric Chemistry Research Group, Chemical Resource Beneficiation, North-West University, Potchefstroom, South Africa, [3]Department of Technical Physics, University of Eastern Finland, Kuopio, Finland, [4]Joint Mass Spectrometry Centre, Comprehensive Molecular Analytics, Helmholtz Zentrum München, Neuherberg, Germany, [5]Now at Analytical Chemistry Group, Department of Plant and Environmental Sciences, Faculty of Science, University of Copenhagen, Copenhagen, Denmark, [6]Department of Environmental and Biological Sciences, University of Eastern Finland, Kuopio, Finland, [7]Department of Environmental and Biological Sciences, University of Eastern Finland, Joensuu, Finland, [8]Joint Mass Spectrometry Centre, Chair of Analytical Chemistry and Department Life, Light & Matter, University Rostock, Rostock, Germany, [9]Now at Aerodyne Research, Inc., Billerica, MA, USA, [10]Unit for Environmental Sciences and Management, North-West University, Potchefstroom, South Africa, [11]Department of Chemistry and Sustainable Technology, University of Eastern Finland, Joensuu, Finland

Key Points:

- Organic aerosol and volatile organic compound emission factors increased linearly with decreasing modified combustion efficiency
- Aerosol particle size distributions and optical properties depended on combustion characteristics
- O:C ratio of primary organic compounds was affected by biomass type

Supporting Information:

Supporting Information may be found in the online version of this article.

Correspondence to:

V. Vakkari,
ville.vakkari@fmi.fi

Citation:

Vakkari, V., Vettikkat, L., Kommula, S., Mukherjee, A., Hao, L., Backman, J., et al. (2026). Laboratory experiments on savannah and European Boreal forest fire emissions. *Journal of Geophysical Research: Atmospheres*, *131*, e2025JD044543. https://doi.org/10.1029/2025JD044543

Received 6 JUN 2025
Accepted 23 MAR 2026

Abstract Landscape fire is among the largest sources of aerosols and trace gases globally. However, the emissions are highly variable and strongly affected by the type of biomass and combustion characteristics. We investigated the effect of combustion characteristics on the burning emissions from three biomass types: woody plants and grasses from southern African savannah and European boreal forest surface based on experiments at the ILMARI combustion facility in Kuopio, Finland. Considering emission factors (EF) for organic aerosol (OA) and for the sum of volatile organic compounds (VOCs), we observed a linear increase in the EF with decreasing modified combustion efficiency (MCE) down to MCE of 0.6. For instance, for woody plants from savannah flaming combustion EF_{OA} is 6.1 g kg^{-1} at MCE of 0.94, while extreme smoldering EF_{OA} at MCE of 0.67 is 54 g kg^{-1}. Interestingly, the effect of biomass type was minor compared to MCE, which was also seen for aerosol particle number size distributions. Likewise, the absorption Ångström exponent increased with decreasing MCE. Furthermore, OA in our experiments is absorbing not only at the short wavelengths, which is typical of brown carbon, but even at the longest wavelengths (880 and 950 nm), which are often considered to represent only absorption by black carbon. The biomass type impacted the OA and VOC composition, especially in higher O:C ratio for savannah grass emissions, irrespective of combustion characteristics.

Plain Language Summary Landscape fires, such as forest and savannah fires, are among the largest sources of fine particulate matter and trace gases globally. However, the emissions are highly variable and strongly affected by the type of biomass and whether the fire was flaming or smoldering. We conducted laboratory experiments to better characterize the emissions from three biomass types: woody plants and grasses from the southern African savannah and European boreal forest surface. Our experiments indicate that even a relatively small amount of biomass consumed in extreme smoldering conditions can emit substantial numbers of particles and reactive gaseous compounds.

1. Introduction

Open biomass burning (BB), such as forest and savannah fires, is the largest source of carbonaceous aerosol particles, including ca. 40% of the black carbon (BC) emitted into the Earth's atmosphere annually (e.g., Andreae, 2019; Bond et al., 2013). Furthermore, it is the second largest source of VOCs after biogenic emissions (e.g., Akagi et al., 2011; Andreae, 2019). Weather is recognized as one of the main drivers of fire activity and it is, for instance, apparent in the European boreal forest fire history (Aakala et al., 2017). Now, predicted changes in climate are expected to increase weather conditions that are conducive for more widely spread fires throughout the world (e.g., Abatzoglou et al., 2019, 2021). In some regions, such as the western United States, landscape fires

have already become more frequent and have distinct adverse effects on air quality on a sub-continental scale (e.g., Jaffe et al., 2020; O'Dell et al., 2019).

Recently, emissions from landscape fires in North America have received substantial attention, both in terms of several large field measurement campaigns (e.g., Gkatzelis et al., 2024; Hodshire et al., 2019; Lindaas et al., 2021; Warneke et al., 2023) as well as laboratory experiments (e.g., May et al., 2013; Selimovic et al., 2018; Stockwell et al., 2014). In contrast, savannah fires are currently estimated to comprise approximately half of the global open BB emissions (van Wees et al., 2022), but comparatively few studies have focused on the characteristics of savannah fire emissions (Desservettaz et al., 2017; Milic et al., 2017; Stockwell et al., 2015; Vakkari et al., 2014, 2018; Vernooij et al., 2022, 2023; Wu et al., 2021) after the SAFARI campaigns (H. J. Christian et al., 2003; Yokelson et al., 2003). However, recent studies over the South East Atlantic have observed substantial amounts of savannah fire smoke in this area (Dobracki et al., 2023; Haslett et al., 2019; Wu et al., 2020, 2021), which has the potential for significant climate effects above and inside the marine cloud deck (Che et al., 2022). Long-range transported savannah fire emissions from Africa have been observed even over the Amazon rain forest (Holanda et al., 2020, 2023). Similarly, from the boreal region, fire emissions are readily transported over the Arctic (e.g., Kommula et al., 2024), where they may deposit on snow and ice, accelerating melting and decreasing the surface albedo (McCarthy et al., 2021).

Open BB emissions are known for their variability, especially, in terms of EF, which indicates the mass emission of for example, OA, particulate matter <2.5 μm in diameter (PM2.5) or VOC per burned kilogram of biomass (e.g., Akagi et al., 2011). Differences in the biomass type and the combustion process (essentially the ratio of flaming vs. smoldering combustion) are considered as main drivers of this variability, and EFs are primarily presented as vegetation type averages (e.g., Akagi et al., 2011; Andreae, 2019; Binte Shahid et al., 2024). Among the different vegetation types considered by Andreae (2019), the savannah presents the lowest average $EF_{PM2.5}$ of 6.7 g kg^{-1}, while temperate forest, boreal forest and peat fires exhibit the highest average $EF_{PM2.5}$ of 18.5, 18.7 and 18.9 g kg^{-1}, respectively. There is substantial heterogeneity within the vegetation types, though. For instance, high intensity crown fires are dominant in North American boreal forests, while European boreal forest fires are typically of lower intensity and often consume only the surface layer vegetation (Köster et al., 2024; Rogers et al., 2015; Shorohova et al., 2011). To our knowledge, aerosol particle and VOC EFs from European boreal forest surface fires have not been previously quantified.

Compared to vegetation type effects, fewer studies have focused on quantifying the effect of combustion characteristics on fresh aerosol and VOC emissions (Gkatzelis et al., 2024; Jen et al., 2019; Vernooij et al., 2022; Yokelson et al., 2011) or their aging (Vakkari et al., 2014, 2018). It is well known though that the EF for both particulate and gas phase compounds, with relatively few exceptions such as BC, present a decreasing trend with increasing flaming fraction in the fire (e.g., Gkatzelis et al., 2024; Jen et al., 2019; Vakkari et al., 2018; Yokelson et al., 2011). Combustion is typically characterized through MCE, that is, the ratio of CO_2 to sum of CO_2 and CO emissions (e.g., Akagi et al., 2011). For purely flaming combustion, MCE approaches 1, while 0.9 is considered to represent half-flaming, half-smoldering combustion (e.g., Akagi et al., 2011). For example, Vernooij et al. (2022) reported that savannah fire $EF_{PM2.5}$ decreased from ca. 17 g kg^{-1} at an MCE of 0.85 (smoldering-dominated combustion) to ca. 2.5 g kg^{-1} at an MCE of 0.97 (i.e., flaming-dominated combustion). Only recently has the variability in EFs been included in an emission inventory (Vernooij et al., 2023).

In 2022, we carried out a laboratory campaign "Boreal and savannah fire aerosol aging" (BASFAA) at the ILMARI combustion facility in Kuopio, Finland. The BASFAA campaign was designed to characterize the effect of combustion characteristics on particulate and VOC emissions and their aging in an atmospheric simulation chamber for three relatively under-studied biomass types: woody plants and grasses sourced from a grassland savannah environment in South Africa and European boreal forest surface layer samples collected in Finland. In this paper, we focus on the characterization of the primary emission properties including particulate and VOC EF, chemical composition, volatility, refractive BC (rBC) and aerosol particle number size distributions, as well as aerosol particle optical properties. The effect of combustion characteristics on these parameters is quantified and compared for the three different biomass types based on 27 experimental burns. Our results also provide a starting point for ongoing analysis of the BASFAA data, which includes cloud condensation nuclei and ice nuclei activity of the aerosol, photochemical and dark aging effects on the aerosol including brown carbon (BrC) evolution, and more detailed chemical characterization of the emissions with novel methodologies.

Table 1
Overview of BASFAA Experiments Including Observed MCE, Dilution Factor and Primary OA (POA) Concentration in the Chamber

Date	Biomass	MCE	Dilution factor	POA [μg m^{-3}]	Aging	Comment
03 May 2022	savannah wood			46.4	UV light + O_3	Smoldering-dominated 2 batches combusted
04 May 2022	savannah wood			44.1	UV light + O_3	Smoldering-dominated
05 May 2022	savannah wood		70	3.0	UV light + O_3	Smoldering-dominated
06 May 2022	savannah grass	0.756 ± 0.005	180	16.1	UV light + O_3	Glowing after flaming
09 May 2022	savannah grass	0.943 ± 0.001	490	21.4	UV light + O_3	
10 May 2022	savannah grass	0.803 ± 0.004	580	5.7	UV light + O_3	Glowing after flaming 2 batches combusted
11 May 2022	blank		160	0.0	UV light + O_3	No combustion
12 May 2022	savannah grass	0.852 ± 0.002	4260	7.1	UV light + O_3	
13 May 2022	savannah grass	0.969 ± 0.0005	1900	5.0	UV light + O_3	2 batches combusted
16 May 2022	savannah grass	0.952 ± 0.001	840	26.2	UV light + O_3	
17 May 2022	savannah wood	0.589 ± 0.055	380		UV light + O_3	2 batches combusted
19 May 2022	savannah wood	0.886 ± 0.003	440	23.0	UV light + O_3	
20 May 2022	savannah wood	0.858 ± 0.005	440	20.3	UV light + O_3	
23 May 2022	savannah wood	0.929 ± 0.001	1030	12.7	UV light + O_3	
24 May 2022	savannah wood	0.935 ± 0.001	800	29.8	UV light + O_3	
25 May 2022	boreal forest surface	0.763 ± 0.009	140	41.6	UV light + O_3	
27 May 2022	boreal forest surface	0.741 ± 0.012	90	43.2	UV light + O_3	
30 May 2022	boreal forest surface	0.702 ± 0.015	300	30.2	UV light + O_3	
31 May 2022	savannah wood	0.672 ± 0.022	350	32.0	O_3	
01 Jun 2022	savannah wood	0.950 ± 0.001	200	16.1	O_3	
02 Jun 2022	savannah wood	0.892 ± 0.002	340	47.1	O_3	
03 Jun 2022	savannah grass	0.843 ± 0.002	770	38.3	O_3	
06 Jun 2022	savannah grass	0.973 ± 0.0004	1590	19.7	O_3	
07 Jun 2022	savannah grass	0.895 ± 0.002	290	49.9	UV light + O_3	2 batches combusted
08 Jun 2022	boreal forest surface	0.743 ± 0.006	290	52.6	O_3	
09 Jun 2022	boreal forest surface	0.839 ± 0.003	310	15.2	UV light + O_3	
10 Jun 2022	boreal forest surface	0.758 ± 0.009	170	22.5	O_3	

Note. In five cases, a second batch of biomass was combusted as the POA concentration in the chamber was found lower than desired after the first feeding.

2. Materials and Methods

The BASFAA campaign took place at the University of Eastern Finland ILMARI facility in Kuopio, Finland from May to June 2022. In total, 27 experiments with three types of biomass were carried out during the BASFAA campaign as listed in Table 1. The experiment on 11 May 2022 was a blank experiment, where the experimental procedure was followed exactly as on actual BB days, but no biomass was combusted. No background aerosol, primary or secondary, was observed during the blank experiment (Figure S1 in Supporting Information S1). The other 26 experiments comprised 6 experiments with boreal forest surface from Finland, 11 experiments with woody material from a savannah in South Africa, and 9 experiments with grassy material from a savannah in South Africa.

To study the aging of these emissions, the smoke was injected into an environmental chamber with the majority of measurements taken from this chamber. Although this study only focussed on fresh emission characterization with a sub-set of the on-line methods, the full set of instrumentation is introduced in this paper.

2.1. Biomass Types and Combustion Setup

As previously mentioned, BB experiments with three types of biomass were carried out in the BASFAA campaign. In South Africa, woody plants and grasses were collected from a grassland savannah environment near a Welgegund atmospheric measurement station (e.g., Jaars et al., 2016). Woody material from South Africa (hereafter savannah wood) consisted of branches of *Asparagus laricinus, Celtis africana, Euclea undulata, Gymnosporia buxifolia, Pavetta zeyheri, Searsia pyroides, Senegallia caffra, Vachellia erioloba, V. karroo, Vangueria infausta, Zanthoxylum capense* and *Ziziphus mucronata.* Grasses from South Africa (hereafter savannah grass) consisted of *Anthephora pubescens, Cymbopogon caesius, Cynodon dactylon, Digitaria argyrograpta, Elionurus muticus, Eragrostis chloromelas, E. lehmanniana, Heteropogon contortus, Setaria sphacelata* and *Themeda triandra.* Dried leaf litter was not included although it can form >25% above-ground fuel load in some savannah environments (Shea et al., 1996). European boreal forest surface samples were collected from an experimental fire area (Köster et al., 2024), located in an even-aged 75-year-old Scots pine stand. The samples (Ø = 0.21 m) consisted of the topmost vegetation and soil layers (vegetation, litter, and the soil organic layer).

For the experiments with savannah wood and -grass, the sample was mixed in order to contain all above-mentioned species for each burn in approximately equal mass. However, in none of the experiments, grasses and woody material from the savanna burned together. The average weight of the biomass burned was 60 g for the savannah wood experiments, 50 g for the savannah grass experiments and 500 g for the boreal forest surface experiments. The moisture content of the biomass was 9.4% for savannah wood, 8.6% for savannah grass and 9.6% for boreal forest surface, representing dry conditions. The carbon content was 48.8% for savannah wood, 43.0% for savannah grass and 42.8% for boreal forest surface. Moisture content and elemental composition of the three biomasses were analyzed at an accredited laboratory (Eurofins Environment Testing Finland Oy) and are presented in Table S1 in Supporting Information S1.

Combustion took place under an open stack mimicking natural burning and dilution similar to T. J. Christian et al. (2004), though in a smaller size, where the fuel bed was approximately 50 cm in diameter. For the combustion, savannah wood and grass were placed upright in a wire mesh sample holder 6 cm in diameter. Boreal forest floor samples were placed in a wire mesh sample holder 23 cm in diameter. The biomass samples were ignited with a resistor heating element, for which the temperature was controlled with an adjustable power supply. The sample was injected from the stack into a 29 m^3 environmental chamber (Leskinen et al., 2015) with a two-stage dilution system, including a porous tube diluter followed by an ejector diluter (Tiitta et al., 2016). Purified air supplied by Woikoski Oy was used in the diluters, as it was found that the CO_2 concentration of the on-site purified air system (Aadco Instruments Inc. Model 737-250) varies over time. The effects of the CO_2 variability of purified air are discussed in more detail in Section 2.3. The environmental chamber was filled with particle and trace gas free air generated on site with the purified air system and flushed overnight before each experiment. The layout of the instrumentation at the ILMARI facility was similar to Tiitta et al. (2016) and a schematic drawing of the setup is presented in Figure S2 in Supporting Information S1. In this study, we utilize only instruments connected to the chamber, but additionally an FTIR analyzer (Gasmet Technologies Inc.) as well as CO and CO_2 analyzers were connected directly to the undiluted smoke in the stack. A list of instrumentation is included in Table S2 in Supporting Information S1.

The dilution of the sample was designed to represent fast dilution of emissions in a convective boundary layer leading to POA concentrations varying from approx. 5 to 50 μg m^{-3} (Table 1), which aligns with the majority of savannah and grassland fire plumes observed at the Welgegund measurement station in South Africa (Vakkari et al., 2018). Plume age at Welgegund varies from 15 min to approx. 5 hr (Vakkari et al., 2018). We consider this a realistic dilution also for boreal forest surface fires. We have estimated the dilution factor as

$$\text{dilution factor} = \frac{V_{\text{chamber}} + V_{\text{ejectors}} + V_{\text{sample}}}{V_{\text{sample}}}, \quad (1)$$

where V_{chamber} is estimated to be 28 m^3, as the chamber was kept a little short of full at the start of feeding to make sure that the sample feeding will fit in it, $V_{\text{ejectorrs}}$ is the volume of the dilution air in the ejector and porous diluters, and V_{sample} is the volume of air injected from the stack into the chamber. For the two first experiments, the ejector and porous dilutor settings were not saved, and dilution factor cannot be estimated. Dilution factors for all other

experiments are included in Table 1. Relative humidity (RH) in the chamber was set to 20% for savannah experiments and to 50% for boreal forest surface experiments to reflect typical daytime RH in each environment during the fire active season, respectively.

To cover a wide range of combustion characteristics for each biomass, we varied the timing of the sample injection into the environmental chamber with respect to the time of ignition of the sample. During sample injection, a fast mobility particle sizer (FMPS; TSI model 3091) was connected to the feeding line after the ejector diluters to enable real-time estimation of the submicron particulate mass injected into the chamber.

2.2. Measurements

A 15-min period before sample injection was used to quantify chamber background and was subtracted from the measurements in the analysis. After the sample was injected into the environmental chamber and had mixed evenly in the chamber, as indicated by a stable rBC number concentration, a 45-min period of primary measurements commenced. Thereafter, deuterated butanol was injected into the chamber, followed by oxidants, similar to Tiitta et al. (2016). Aging experiments were carried out both under dark conditions, when only O_3 was injected, and with UV-lights on, when additional H_2O_2 was injected to generate OH• in the chamber. For dark experiments, O_3 concentration at the beginning of the aging experiment was approx. 100 ppb. For UV-light experiments, O_3 concentration at the beginning of the aging experiment was approximately 50 ppb, representing regional background concentration. The aging continued for 4.5 hr of wall time after the injection of oxidants was completed. During the UV-light on experiments, a photochemical age of approx. 24 hr was reached. However, in this paper, we focus only on the primary emissions. For completeness, we next introduce all measurements from the environmental chamber.

2.2.1. CO_2, CO and CH_4

A Picarro G2401 analyzer was used to quantify CO_2, CO and CH_4 in the chamber before and after sample injection. During the sample injection, the Picarro was connected directly after the ejector diluters to measure the sample being injected into the chamber. Before each experiment, the Picarro was also used to measure room air concentrations next to the combustion platform. After the first three experiments, it was found that the CO_2 concentration in the purified compressed air system varied during sample injection. Therefore, on 5 May 2022 the Picarro was used to also measure purified air immediately before and after the sample injection. After that, purified air from the cylinders was used for ejector diluters, while cylinder concentrations were measured using the Picarro every time there was a change.

The Picarro was calibrated before and after the BASFAA campaign according to the Integrated Carbon Observation System protocol at the Finnish Meteorological Institute, Greenhouse Gas research group. Calibration-corrected readings were used in MCE and EF calculations. The 5-s time resolution precision for Picarro CO_2, CO and CH_4 are <50 ppb, <15 ppb and <1 ppb, respectively (Picarro Inc., 2021).

2.2.2. VOCs

A Vocus proton transfer reaction time of flight mass spectrometer (Vocus-PTR; Tofwerk AG, Aerodyne Research Inc., Krechmer et al., 2018) was used for online VOC measurements. We operated the ion-molecule reactor (IMR) at 2.5 mbar pressure, 100°C temperature and an electric field strength of 57.5 V cm^{-1} resulting in a field of 118.5 Townsend (10^{-17} V cm^2). Regular automated single-point calibrations (n = 80) were performed using a calibration standard containing 14 calibration gas standards (Apel Reimer Environmental Inc.). The compounds calibrated with the standards were Ethanol, Acetonitrile, Acetone, Acrylonitrile, Isoprene, Methyl Vinyl Ketone, Methyl Ethyl Ketone, Benzene, m-Xylene, α-Pinene,1,2,4-Trimethylbenzene, siloxanes (D4 and D5) and β-Caryophyllene. The calibration gas contained around 1 ppmv of calibration gas (except for β-Caryophyllene at 100 ppbv) and was diluted with zero air from a zero-air generator (Tofwerk AG) to reach a target mixing ratio of 4 ppbv for the single-point calibrations. The instrument zeros were performed regularly for 30 s every 15 min. Zeros were linearly interpolated and subtracted from the measured data.

For Vocus, the maximum sensitivity was observed for acetone and was used as the sensitivity factor for calibrating all ions with the exception of the calibrant compounds. Hence, the reported ppbv values give the lower limit of measurements. All detected and identified ions (n = 466) excluding the primary ions ($(H_2O)_nH^+$) and ions

containing deuterated hydrogen (^{2}H), silicon (Si) and fluorine (F) were used for further analysis. Fragmentation inside the Vocus-PTR was not taken into consideration. The propagation of errors in instrument precision, VOC calibration gas mixing ratio (5%), and MFCs (1% each) used for dilution were also utilized to calculate the uncertainties and an uncertainty of 7.2% was observed for acetone. Therefore, we estimate the uncertainty in the sum of VOC concentrations from the Vocus to be 10%, which is in line with Jensen et al. (2023).

2.2.3. Aerosol Particle Chemical Composition

Size-resolved chemical composition and mass concentration of submicron non-refractory aerosol particles were measured with an online high-resolution time-of-flight aerosol mass spectrometer (HR-ToF-AMS, hereafter AMS) (DeCarlo et al., 2006). The bulk aerosol particles are identified as non-refractory chemical species, including organics, sulfate, nitrate, ammonium and chloride. The AMS was calibrated on-site with ammonium nitrate and ammonium sulfate aerosols. In this campaign, AMS was operated in EI-V mode (tungsten vapourizer). The default values of relative ionization efficiency (RIE) of 1.0 and 1.3 were used for quantification of nitrate and chloride. The RIEs for ammonium and sulfate were determined to be 3.5 and 1.35, respectively. The default RIE for OA is 1.4, determined using laboratory-derived organic surrogates (Jimenez et al., 2003, 2016). Recent studies have shown that RIE_OA may be associated with the organic OSc state (Xu et al., 2018) and the fractional contribution ions less than m/z50 (hereafter referred to as $f_{\sum m/z50}$) (Nault et al., 2023). In this study, OSc in the primary emission phase ranges from −0.3 to −1.49. The $f_{\sum m/z50}$ values for savannah wood, savannah grass and boreal forest surface experiments are 47%, 58% and 41%, respectively. In addition to RIE, CE also contributed to an uncertainty of quantification. Particularly during the aging phase, the formation of oxidized organic compounds not only increases RIE but also alters the particle phase, resulting in a decrease in CE (Docherty et al., 2013; Lim et al., 2019). Considering the uncertainties of RIE and CE, we use the term RIE × CE to reflect the potential variations in RIE and CE of OA particles due to the complexity of combustion aerosols. The RIE × CE for organic matter during the primary emission stage was estimated to be in a range of 0.8–1.4, and RIE × CEs for the secondary organic aerosol formation stage were in a range of 0.7–0.9. Using these values, AMS derived aerosol volume concentrations are consistent with those obtained by SMPS (slope = 0.97, $r^2 = 0.86$). The elemental ratios of O:C and H:C were determined using the improved ambient parametrization (Canagaratna et al., 2015).

Refractory BC (rBC) size distributions were measured with a single-particle soot photometer (SP2). The SP2 is a single particle instrument that detects the amount of rBC in single particles, on a particle-by-particle basis. In this work, we only use the broad band detectors to determine the mass of the rBC particles. SP2 broad band incandescent detector was calibrated on-site with Aquadag and a differential mobility analyzer (DMA). Eight sizes were selected with the DMA, ranging from 70 to 400 nm in size. DMA-selected diameters were converted into particle mass based on the effective density parametrization of Aquadag by Gysel et al. (2011). The SP2 scattering detector was calibrated on-site with 269 and 300 nm PSL particles. SP2 data were post-processed using the PySP2 Python package (https://github.com/ARM-DOE/PySP2, version 1.5). Since the concentrations during the experiments were high, the deadtime correction by Schwarz et al. (2022) was used to correct the SP2 data. The deadtime correction is also a part of the PySP2 python package.

Additionally, a Filter Inlet for Gases and AEROsols (FIGAERO, Lopez-Hilfiker et al., 2014; Bannan et al., 2019; Ylisirniö et al., 2021) coupled with a time-of-flight chemical ionization mass spectrometer (ToF-CIMS, Tofwerk AG, Aerodyne Research Inc.) with mass resolution of 4000–5000 was deployed during the BASFAA campaign. FIGAERO-CIMS was operated with an iodide-ionization scheme (B. H. Lee et al., 2014), where iodide ions were generated by passing 1 standard liter per minute (LPM) of ultrapure nitrogen (N_2) over a permeation tube containing methyl iodide (CH_3I) and through a commercial Po-210 source (Model P-2021, NRD Static Control LLC) into the IMR of the instrument. The IMR was operated at a pressure of 100 mbar, which was actively controlled.

The FIGAERO inlet enables measurement of both gas- and particle phase constituents. However, in this paper we utilized only the particle phase data from the FIGAERO and therefore only details related to particle phase sampling are discussed. The operation principle of FIGAERO particle phase sampling is more thoroughly described in earlier publications (Bannan et al., 2019; Lopez-Hilfiker et al., 2014; Ylisirniö et al., 2021). Briefly, in a typical particle phase measurement cycle, aerosol particles are collected onto a PTFE filter while the instrument is measuring the gas phase. Once the collection is done, the filter is moved in front of a 2 LPM pin hole leading into the instrument and gradually heated ultrapure N_2 is passed through the filter into the instrument.

While comparing the ions measured by the CIMS with the temperature of the N_2 flow, one can construct a so called thermogram for each ion (ion count rate vs. desorption temperature). The shape of a typical thermogram is lognormal-like. The maximum of the thermogram is called T_{max}, which, with proper calibration, can be used to estimate the effective saturation vapor pressure of the desorbing molecule (Ylisirniö et al., 2021). During BASFAA, aerosol particles were collected with sampling flows varying from 1 to 4 LPM and sampling times varying from 5 to 30 min, depending on the particle mass concentration in the ILMARI chamber, as measured by SMPS and AMS. Thereby, variations in the collected mass on the FIGAERO filter for each measurement cycle were limited to 400–700 ng. In a typical experiment day, the filter was initially desorbed twice without collecting particles to it. One sample was then collected and desorbed from the fresh emissions, before oxidants were fed into the chamber. After that, the instrument measured normally alternating between gas and particle phase measurements until the end of the experiment.

The FIGAERO volatility range was calibrated by collecting polyethylene glycol particles atomized from an acetonitrile solution following the procedure described by Ylisirniö et al. (2021). The used PEGs were of polymer size 5–8. T_{max} values of these compounds were used to acquire fit parameters a and b of equation

$$\ln(P_{sat,lit}) = aT_{max} + b, \quad (2)$$

where $P_{sat,lit}$ is the literature saturation pressure values of the PEGs (Krieger et al., 2018). The determined fit values were $a = -4.2116$ and $b = -0.1642$.

A novel instrument for single-particle mass spectrometry (SPMS; PhotonLIZA, Photonion GmbH, Germany) was utilized for real-time characterization of individual particles, including polycyclic aromatic hydrocarbons (PAHs) (Schade et al., 2019). Particles are optically detected, sized and subsequently exposed to laser pulses for ion formation, with a bipolar time-of-flight mass analyzer detecting both anions and cations to generate chemical profiles of individual particles. The instrument employs a novel laser excitation approach, using a combination of laser desorption/ionization for refractory and inorganic components and laser desorption/resonance-enhanced multiphoton ionization for PAHs. For further details, see Schade et al. (2019). While single-particle mass spectrometry does not provide absolute mass concentrations, it offers valuable chemical insights at the individual particle level, facilitating comparative studies and identifying characteristic chemical patterns.

2.2.4. Aerosol Particle Physical Properties

Aerosol particle number size distribution was measured using a scanning mobility particle sizer (SMPS; TSI model 3082) at 3 min time resolution. The size range of the SMPS was from 14.6 to 685 nm with 108 size bins. A second SMPS was combined with an Aerosol Particle Mass analyzer (APM; Kanomax model 3602) for aerosol particle effective density analysis.

Aerosol particle scattering and backscattering coefficients (b_{scat} and b_{bsca}) were measured with an AirPhoton IN102 integrating nephelometer at three wavelengths of 450, 532 and 632 nm. Nephelometer flow rate was 3.0 LPM and time resolution was 1 min. Nephelometer calibration was checked six times during the campaign with CO_2 and a HEPA filter. During the campaign, a minor drift was identified in the calibration coefficients, which was accounted for with a linear fit to the calibration coefficients. Integrated scattering- and backscattering coefficients were corrected in this manner. Truncation correction was performed according to the instrument manual, that is, using the Müller et al. (2011) method with TSI nephelometer coefficients. Uncertainty in b_{scat} is estimated to be 5% (Müller et al., 2011).

Aerosol particle absorption coefficient (b_{abs}) was measured using a seven wavelength aethalometer (Magee Scientific model AE-42) at 2 min time resolution. A fresh filter spot was advanced for each experiment. Aethalometer output was converted from mass into absorption coefficient with the Magee BC mass absorption coefficient $14625/\lambda$, where λ is the wavelength in nanometers. The aethalometer wavelengths were 370, 470, 520, 590, 660, 880 and 950 nm. Aethalometer absorption coefficients were corrected for the filter loading artifact with the Collaud Coen et al. (2010) algorithm, using $C_{ref} = 3.5$. Uncertainty in b_{abs} is estimated to be 35% (Zanatta et al., 2016).

For the Collaud Coen et al. (2010) algorithm, the scattering Ångström exponent was calculated as the negative slope from a least-squares fit to the logarithm of scattering coefficient versus the logarithm of the wavelength at

the three nephelometer wavelengths. The scattering Ångström exponent is then used to extrapolate b_{scat} to the aethalometer wavelengths with the single scattering albedo (SSA) then calculated as

$$SSA(\lambda) = \frac{b_{scat}(\lambda)}{b_{scat}(\lambda) + b_{abs}(\lambda)}. \quad (3)$$

In addition to the Collaud Coen et al. (2010) algorithm, SSA merits study also as such as it determines whether particles heat or cool the atmosphere, that is, the direct radiative forcing by aerosols. For uncoated pure BC, SSA is approx. 0.2 ± 0.1 (Bond et al., 2013) and clearly higher for other aerosol types.

The aerosol particle absorption coefficient is approximately proportional to the power function $b_{abs} \propto \lambda^{-AAE}$, where absorption Ångström exponent (AAE) is the AAE. It is frequently used to distinguish absorbing aerosol types: for pure BC particles AAE is approx. 1, while for other light absorbing aerosols (e.g., BrC, mineral dust) it is clearly >1 (e.g., Bond et al., 2013; Zotter et al., 2017). Here, AAE is calculated from a least-squares fit to the logarithm of b_{abs} versus the logarithm of the wavelength, similar to the scattering Ångström exponent. AAE was calculated for three wavelength ranges: 370–950, 370–520 and 520–950 nm. Uncertainty in SSA and AAE is calculated from instrumental uncertainty with Gaussian error propagation assuming uncorrelated errors.

The mass absorption coefficient for rBC (MAC_{rBC}) is defined for the aethalometer wavelengths as

$$MAC_{rBC}(\lambda) = \frac{\Delta b_{abs}(\lambda)}{\Delta rBC}, \quad (4)$$

where Δ indicates that the chamber background was subtracted from both rBC and b_{abs}. Uncertainty in MAC_{rBC} is calculated through Gaussian error propagation assuming uncorrelated errors.

2.3. Determining MCE and EF

In the BASFAA campaign, it was originally envisaged to determine MCE and EFs based on CO_2, CO and VOCs measured in the stack with an FTIR system. However, the FTIR was not sensitive enough for the relatively low concentrations in the stack during this campaign. Therefore, the smoke CO_2, CO and CH_4 concentrations are determined from the diluted smoke as it is being fed into the environmental chamber using on-line measurement with a Picarro G2401 analyzer.

Given the 5 s time resolution of the Picarro, we considered the possibility of missing rapid changes in the CO_2, CO and CH_4 concentrations in the smoke. Therefore, we also collected a bag sample from the same sampling point where the Picarro was connected for the duration of the sample feeding and analyzed it later with the same Picarro. From this comparison, we estimate that the uncertainty in the CO_2, CO and CH_4 concentrations from online measurement during sample feeding is 1%. For Picarro measurements of in-chamber concentrations and dilution air, we used the stated 5-min uncertainties of 20, 1.5 and 0.5 ppb for CO_2, CO and CH_4, respectively (Picarro Inc., 2021). For room air concentrations, we use the standard deviation of the concentration during the measurement as the uncertainty.

For the first 5 experiments (Table 1), purified compressed air was used to operate the diluters, which feed the sample from the stack to the chamber (Tiitta et al., 2016). The compressed air cleaning system removes particles and trace gases efficiently, with the exception of CO_2. An additional complication is that the concentration of CO_2 varies in the compressed air over time. Therefore, from 10 May onwards, cylinder air was used to operate the diluters. For 6 and 9 May experiments the compressed air CO_2 concentration was measured immediately before and after feeding, and the dilution air CO_2 concentration was linearly interpolated. For these two experiments, the uncertainty in dilution air CO_2 is estimated to be twice as high as for other experiments.

MCE is calculated (e.g., Akagi et al., 2011) by

$$MCE = \frac{\Delta CO_2}{\Delta CO_2 + \Delta CO}, \quad (5)$$

where ΔCO_2 and ΔCO are in parts per million (ppm) with Δ indicating that the dilution and room air contributions have been subtracted. EFs are calculated using the carbon mass balance method (Ward & Radke, 1993; Yokelson et al., 1999) as follows

$$EF_X = F_C \cdot 1000 \cdot \frac{ER_X}{\sum \frac{\Delta C}{\Delta CO}}, \quad (6)$$

where X denotes the compound for which the EF is evaluated. In Equation 6, ER_X is the mass emission ratio of compound X with respect to CO and F_C is the fuel carbon mass fraction. $\sum\Delta C$ includes carbon released in the combustion as CO_2, CO and CH_4 (measured by Picarro), organic carbon (OC, measured by AMS), rBC (measured by SP2) and the carbon contained in VOCs (C_{VOC}, measured by Vocus):

$$\sum \Delta C = \Delta CO_2 + \Delta CO + \Delta CH_4 + \Delta OC + \Delta rBC + \sum \Delta C_{VOC}. \quad (7)$$

Uncertainty in EF_X (σEF_X) is calculated through error propagation assuming 20% uncertainty in OC, 10% uncertainty in rBC and 10% uncertainty in the sum of VOCs from Vocus. More details on the EF calculation and error propagation are included in Supporting Information S1.

3. Results and Discussion

For the first three experiments conducted in the BASFAA campaign with savannah wood (3–5 May 2022), MCE and EFs could not be determined due to difficulties in CO_2 and CO measurements, as detailed in Section 2.3. For these experiments, the sample fed into the chamber was dominated by smoldering phase emissions, but they were excluded from further analysis in this study. On two of the savannah grass experiments, that is, on 6 and 10 May 2022, the sample fed into the chamber consisted of emissions from the glowing and/or smoldering phases of the fire after most of the biomass had been combusted in the flaming phase of the fire. These experiments are termed glowing combustion in further discussion. For all other experiments, the sample fed into the chamber consists of a variable mixture of flaming and smoldering emissions as reflected by the variance of the MCE (Table 1).

3.1. Emission Factors

Considering all experiments collectively, EF_{OA} presents a decreasing trend (correlation coefficient $r = -0.56$) with increasing MCE (Figure 1a). Higher EF with a more smoldering fire (i.e., lower MCE) is a well-known feature in open BB emissions (e.g., Collier et al., 2016; Janhäll et al., 2010; Vakkari et al., 2018; Vernooij et al., 2022). Due to the semi-volatile nature of BBOA, total OA concentration (i.e., dilution) and temperature have a substantial effect on OA partitioning into particle phase and subsequently EF_{OA} retrieval, especially for plumes above the boundary layer (Pagonis et al., 2023). Interestingly, very little difference is observed in the EF_{OA} for the two savannah biomasses for the flaming-dominated experiments (MCE > 0.90). For instance, at MCE of 0.950 ± 0.001 savannah wood EF_{OA} is 6.3 ± 1.8 g kg^{-1} and at MCE of 0.952 ± 0.001 savannah grass EF_{OA} is 6.8 ± 1.7 g kg^{-1}. In this MCE range, the BASFAA savannah EF_{OA} are very close to atmospheric observations of EF_{PM1} (Vakkari et al., 2018) and $EF_{PM2.5}$ (Vernooij et al., 2022) determined in South African savannahs. Also, the flaming-dominated savannah grass and wood experiments (Table 2) agree well with current literature values: $EF_{PM2.5}$ 6.7 ± 3.3 g kg^{-1} at an MCE of 0.94 (Andreae, 2019) and $EF_{PM2.5}$ 7.17 ± 3.42 g kg^{-1} (Akagi et al., 2011). For OC emissions from the savannah, Andreae (2019) give EF_{OC} 3.0 ± 1.5 g kg^{-1} at an MCE of 0.94 and Akagi et al. (2011) give EF_{OC} 2.62 ± 1.24 g kg^{-1}. Considering the default OA/OC mass ratio of 1.6 used in Andreae (2019), the literature EF_{OC} values suggest average EF_{OA} in the range of 4.2–4.6 g kg^{-1}, which falls within the uncertainty of our flaming-dominated experiment averages in Table 2. Recently, Binte Shahid et al. (2024) recommended higher EF for savannah, though: 16 g kg^{-1} for PM2.5 and 27.3 g kg^{-1} for OA, respectively.

For smoldering-dominated experiments (MCE < 0.90), we observe a higher EF_{OA} for savannah wood experiments compared to savannah grass experiments (Table 2). For both savannah wood and grass, the smoldering-dominated EF_{OA} are 2–7.5 times higher than the average EFs indicated by Akagi et al. (2011) and Andreae (2019) (Figure 1a; Table 2). For MCE ranging from 0.80 to 0.90, the BASFAA laboratory experiments EF_{OA} for savannah grass corresponds well with grassland fire EF_{PM1} observed at Welgegund, South Africa

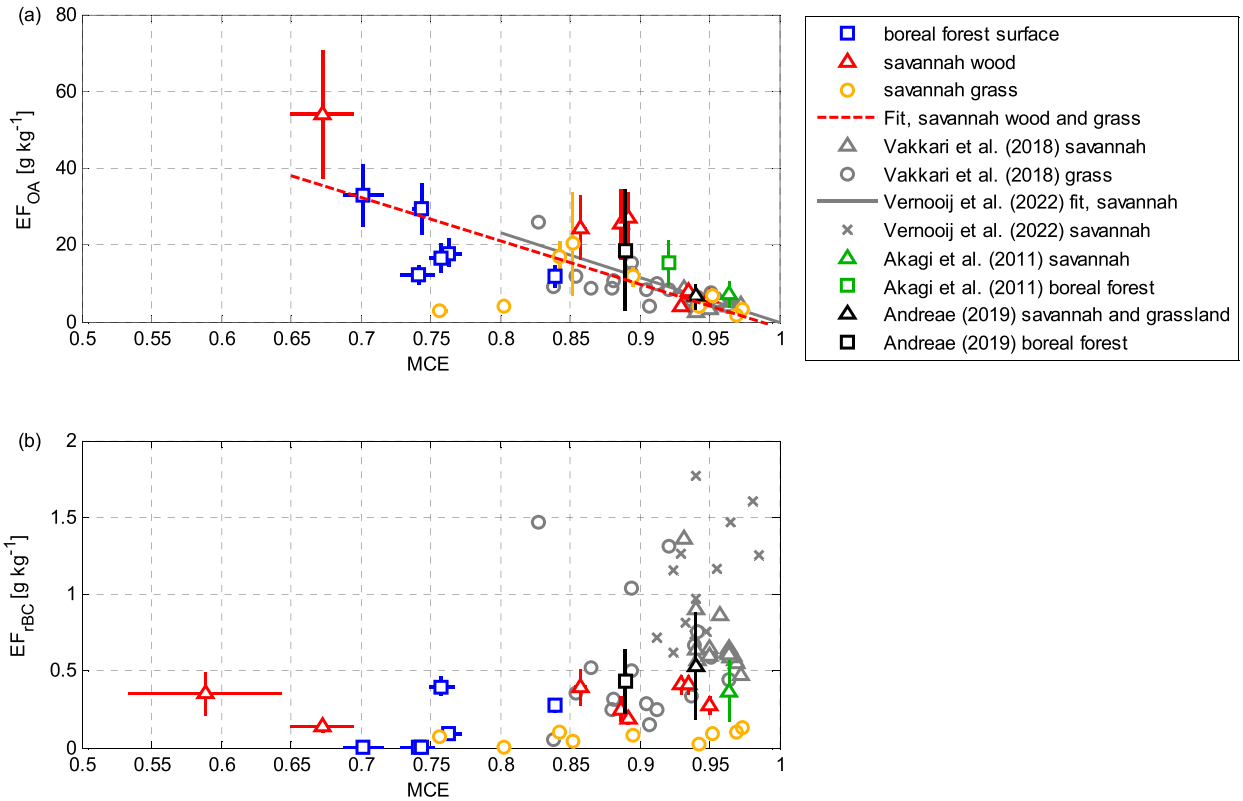

Figure 1. EFs as a function of modified combustion efficiency (MCE) for BASFAA experiments. Error bars indicate measurement uncertainty. Error bars that are not visible are smaller than the size of the marker. (a) EF_{OA} as a function of MCE. Note that the Vakkari et al. (2018) data are for EF_{PM1} and the Akagi et al. (2011), Andreae (2019), and Vernooij et al. (2022) fit are for $EF_{PM2.5}$. (b) EF_{rBC} as function of MCE. Note that the Vakkari et al. (2018) and Vernooij et al. (2022) data are for absorption-based black carbon measurement.

(Vakkari et al., 2018). Savannah wood EF_{OA} in BASFAA experiments for the same MCE range is at the high end of $EF_{PM2.5}$ observations in savannah fires presented by Vernooij et al. (2022), which span from approx. 2 to 40 g kg^{-1} for MCE ranging from 0.80 to 0.90.

In Figure 1a, the two savannah grass experiments with low MCE (0.8 or less) and relatively low EF_{OA} (<5 g kg^{-1}) are clear outliers from the trend of higher EF_{OA} with lower MCE. These two are the experiments where the glowing phase of emissions was measured, that is, the phase after flames had died down, which explains the low EF_{OA} (c.f. Bertschi et al., 2003). We calculated a bivariate linear fit (Cantrell, 2008) for the savannah wood and grass data in Figure 1a, excluding the two glowing phase savannah grass experiments. The resulting fit is $EF_{OA} = -112$ g $kg^{-1} \cdot$ MCE + 111 g kg^{-1}, which is very close to the slope and offset of −116 g kg^{-1} and 116 g kg^{-1}, respectively, in Vernooij et al. (2022) for $EF_{PM2.5}$ as a function of MCE. Our experiments suggest that part of the variability in smoldering savannah fire $EF_{PM2.5}$ observed by Vernooij et al. (2022) may be due to the variable ratio of grasses and woody material consumed in the fire, as well as emissions from the glowing phase of the fire.

For boreal forest surface, the mean (± standard deviation) EF_{OA} in BASFAA experiments is 20 (±9) g kg^{-1}, which is within the range of current literature values for boreal forest: $EF_{PM2.5}$ 18.7 ± 15.9 g kg^{-1} at MCE of 0.89 (Andreae, 2019) and $EF_{PM2.5}$ 15.3 ± 5.9 g kg^{-1} (Akagi et al., 2011). For lower MCE, higher EF_{OA} is again observed (Table 2). However, it should be noted that our boreal forest surface samples did not contain woody material and thus previous EFs for boreal forest cannot be directly compared to the BASFAA experiments. For Alaskan duff, May et al. (2014) report EF_{OA} 27.5 g kg^{-1} at an MCE of 0.900 and for North American coniferous duff Jen et al. (2019) reported EF_{OC} ranging from approximately 20 to 80 g kg^{-1} with MCE ranging from 0.84 to 0.89. Note that OC is only a fraction of OA and thus EF_{OA} and EF_{OC} are not directly relatable. For residual smoldering combustion of North American duff, Bertschi et al. (2003) reported $EF_{PM2.5}$ ranging from 6.6 to 15.1 g kg^{-1} at MCE ranging from 0.848 to 0.879. Considering that residual smoldering combustion results in a

Table 2
Average Particulate Matter EFs for Different Combustion Characteristics and Biomass

Biomass	MCE	EF_{OA} [g kg^{-1}]	EF_{rBC} [g kg^{-1}]	EF_{SO4} [g kg^{-1}]	EF_{NO3} [g kg^{-1}]	EF_{NH4} [g kg^{-1}]	EF_{Cl} [g kg^{-1}]
Boreal forest surface							
Smoldering MCE > 0.80, $N = 1$	0.84 ± 0.003	11.8 ± 2.8	0.28 ± 0.05	0.02 ± 0.006	0.06 ± 0.01	0.000	0.006 ± 0.002
Smoldering MCE < 0.80, $N = 5$	0.74 ± 0.02	21.8 ± 9.0	0.10 ± 0.17	0.04 ± 0.03	0.08 ± 0.04	0.006 ± 0.004	0.012 ± 0.006
Savannah wood							
Flaming MCE > 0.90, $N = 3$	0.94 ± 0.01	6.1 ± 1.9	0.37 ± 0.08	0.06 ± 0.03	0.27 ± 0.04	0.001 ± 0.002	0.12 ± 0.06
Smoldering 0.80 < MCE < 0.90, $N = 3$	0.88 ± 0.02	25.7 ± 1.3	0.30 ± 0.10	0.05 ± 0.002	0.33 ± 0.03	0.003 ± 0.004	0.078 ± 0.009
Smoldering MCE < 0.80, $N = 1$	0.67 ± 0.02	54.2 ± 16.7	0.14 ± 0.04	0.09 ± 0.03	0.78 ± 0.24	0.017 ± 0.005	0.13 ± 0.04
Savannah grass							
Flaming MCE > 0.90, $N = 4$	0.96 ± 0.01	4.0 ± 2.1		0.03 ± 0.003	0.11 ± 0.03	0.002 ± 0.002	0.0072 ± 0.0006
Smoldering MCE < 0.90, $N = 3$	0.86 ± 0.03	16.5 ± 4.4		0.02 ± 0.005	0.26 ± 0.06	0.007 ± 0.007	0.018 ± 0.010
Glowing after flaming $N = 2$	0.78 ± 0.03	3.6 ± 0.9		0.01 ± 0.008	0.10 ± 0.007	0.002 ± 0.002	0.009 ± 0.002

Note. If number of experiments (N) is greater than 1, values are mean and standard deviation. For single experiments, measurement uncertainty is indicated.

lower EF than the EF during the active fire (Bertschi et al., 2003), the previous studies indicate a substantially higher emission factor for North American duff than the European boreal forest surface layer.

For rBC, we find no dependency on EF_{rBC} with MCE ($r = 0.11$; Figure 1b), which is similar to previous studies (e.g., Vakkari et al., 2018; Vernooij et al., 2022). However, for the flaming-dominated experiments (MCE > 0.90) we observe a systematically lower EF_{rBC} than the EF_{BC} observed at the Welgegund measurement site (Vakkari et al., 2018) or by Vernooij et al. (2022). The EF_{rBC} in our experiments, especially, for savannah grass, is suspiciously low at 0.07 ± 0.04 g kg^{-1} on average. For boreal forest surface and savannah wood, we found average EF_{rBC} of 0.13 ± 0.17 g kg^{-1} and 0.30 ± 0.10 g kg^{-1}, respectively. These values are slightly lower than the literature values of 0.43 ± 0.21 g kg^{-1} (Andreae, 2019) reported for boreal forest, as well as 0.37 ± 0.07 g kg^{-1} (Wu et al., 2021), 0.53 ± 0.35 g kg^{-1} (Andreae, 2019) and 0.37 ± 0.20 g kg^{-1} (Akagi et al., 2011) for savannah, respectively. For Alaskan duff, May et al. (2014) reported EF_{rBC} 0.06 g kg^{-1} (at MCE of 0.900), which is within the range of EF_{rBC} we observed for boreal forest surface. Note also that the Welgegund EF_{BC} (Vakkari et al., 2018) is inferred from absorption-based BC measurement with a multi-angle absorption photometer, while here EF_{rBC} is inferred from SP2, which may explain part of the difference. In any case, it is highly likely that in our laboratory setup savannah grass fires are especially less turbulent and possibly not as hot as during a large fire on the field, which leads to lower BC emissions. Therefore, we caution that our savannah grass experiments probably have lower BC than actual grassland fires. Hence, the values are not included in Table 2.

The sum of VOC EFs from the Vocus PTR instrument is shown in Figure 2 as a function of MCE. Here, the negative correlation between the sum of VOC EFs and MCE is much stronger ($r = -0.83$) than for EF_{OA}, while the biomass type appears to have even smaller influence than for EF_{OA}. A bivariate linear fit (Cantrell, 2008) to the data in Figure 2 gives $\Sigma EF_{VOC} = -417\ (\pm 86)$ g kg^{-1} · MCE + 431 (±80) g kg^{-1}. Excluding the two savannah grass experiments that represent the glowing phase of the fire, yields a fit of $\Sigma EF_{VOC} = -829\ (\pm 83)$ g kg^{-1} · MCE + 827 (±79) g kg^{-1}. The strong dependency on MCE is similar to what has been reported for North American BB emissions (e.g., Gkatzelis et al., 2024; Permar et al., 2021). A fit of −565 g kg^{-1} ·MCE + 558 g kg^{-1} has been obtained for the sum of VOC EFs for laboratory experiments on North American BB (Koss et al., 2018; Permar et al., 2021; Stockwell et al., 2015), while for aircraft measurements in North America, lower emissions with slopes of −275 g kg^{-1} (Permar et al., 2021) and −296 g kg^{-1} (Gkatzelis et al., 2024) have been

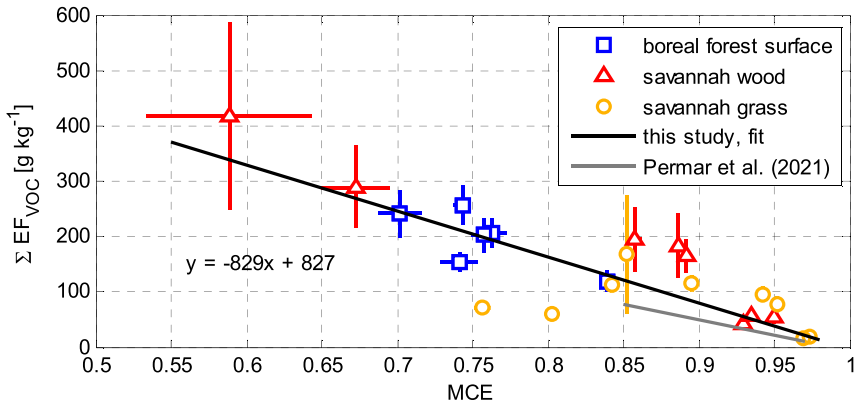

Figure 2. Sum of volatile organic compound EFs from Vocus ptr-tof as a function of modified combustion efficiency for boreal forest surface, savannah wood and savannah grass. Error bars indicate measurement uncertainty. Error bars that are not visible are smaller than the size of the marker. A bivariate fit (Cantrell, 2008) is calculated excluding the two glowing combustion savannah grass experiments. The fit to laboratory experiments from Permar et al. (2021) is also included.

reported. Compared with the North American BB experiments (Permar et al., 2021) and the sum of VOC EFs of 4.5 g kg^{-1} for African grass in Stockwell et al. (2015), our data indicates substantially higher sum of VOC EFs at similar MCE values (Figure 2). However, the sum of VOC EFs for BASFAA experiments is based on 466 ions detected by the Vocus, which is approximately three times as many as included in the fit by Permar et al. (2021). A more detailed analysis of the VOC emissions in the BASFAA experiments is in preparation, including comparison of off-line GC-MS measurements with the online Vocus data.

3.2. Chemical Composition

3.2.1. Aerosol Particles

Based on the AMS and SP2 results, the composition of submicron primary aerosol particles is dominated by OA, as shown in Figure 3. Inorganic species, most importantly, rBC and NO_3, contribute more than 10% of the mass only for flaming-dominated combustion (MCE > 0.90). The major contribution of OA is expected and similar to previous observations (Akagi et al., 2011; Andreae, 2019). For near-source West African savannah fire emissions, Capes et al. (2008) and Wu et al. (2021) reported OA mass fractions of 75% and 85%, respectively. For South Africa, Vakkari et al. (2014) reported 65%–83% OA for relatively fresh savannah and grassland fire emissions, while for Australian savannah fire emissions, Milic et al. (2017) reported 72% contribution by organic compounds. For Alaskan duff, May et al. (2014) reported approx. 95% OA contribution, which is close to what we observed for boreal forest surface. For a boreal forest prescribed burn in Finland, Virkkula et al. (2014) estimated

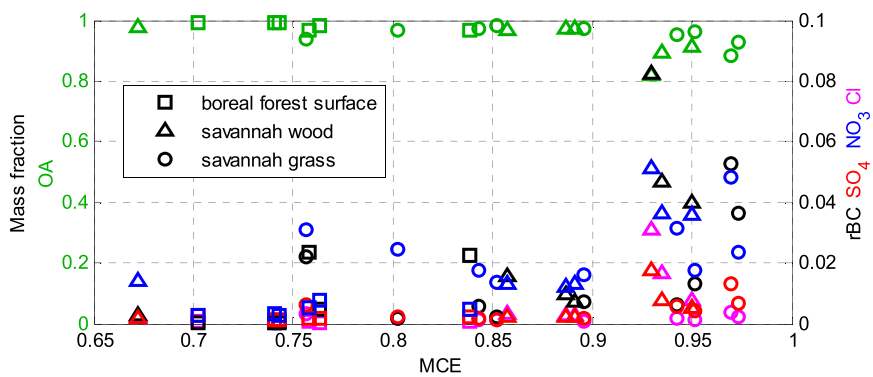

Figure 3. Primary submicron aerosol mass fractions as a function of modified combustion efficiency for the three biomasses in BASFAA experiments. On the left hand side axis organic aerosol and on the right hand side axis rBC, SO_4, NO_3 and Cl. NH_4 mass fraction is at maximum 0.1% and is not plotted.

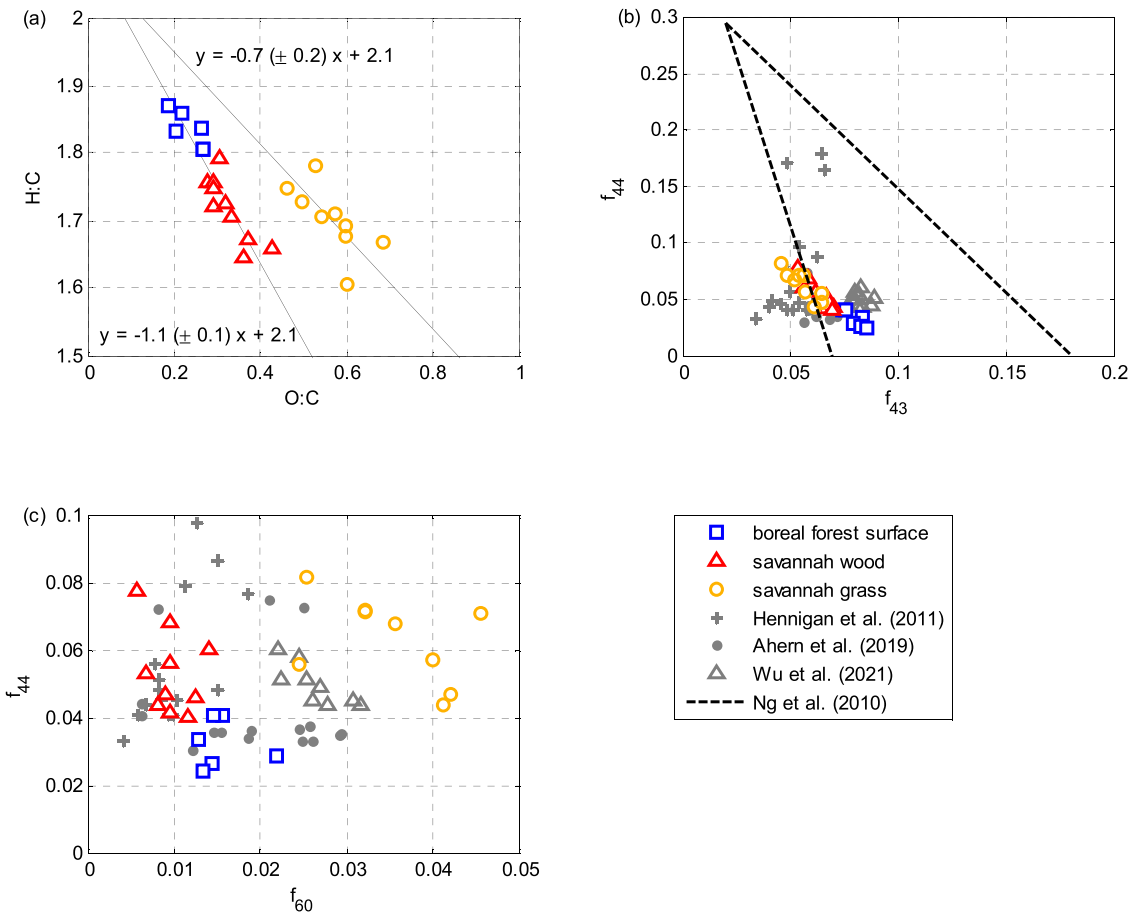

Figure 4. POA properties from AMS measurements for the three biomasses. (a) H:C and O:C ratios. Two linear bivariate fits (Cantrell, 2008) are included: one for boreal forest surface and savannah wood data points combined and another for savannah grass data alone. (b) Fractional signals f_{44} versus f_{43}. (c) Fractional signals f_{44} versus f_{60} (Ng et al., 2010).

approx. 10% BC emission. However, this fire was largely consuming branches and other woody materials, that is, the forest surface had only a minimal contribution to the emission.

For the savannah biomasses, our OA fraction in Figure 3 is a marginally higher than that reported for ambient fire emissions (Capes et al., 2008; Milic et al., 2017; Vakkari et al., 2014; Wu et al., 2021). As noted in Section 3.1, for BASFAA experiments, the savannah grass EF_{rBC} is unrealistically low for flaming fires, and thus also the rBC mass fraction for savannah grass emissions is affected. If the rBC emissions for flaming savannah grass fires are five times higher under ambient conditions than in our experiments, that is, approximately the difference in EF_{BC} in Figure 1b, the rBC mass fraction for savannah grass emissions would be at a maximum of 22% and the OA fraction would be at a minimum of 73%, respectively.

The H:C ratio ranges from 1.6 to 1.9 when considering the AMS OA (Figure 4a), which is in good agreement with previous observations for BB OA that ranges from 1.5 to 1.9 (e.g., Chen et al., 2015; Fortner et al., 2018; J. Y. Lee et al., 2023). We observe a range from 0.2 to 0.7 for the O:C ratio, while previous observations only rarely exceed 0.4 for primary BB OA (e.g., Chen et al., 2015; Fortner et al., 2018; J. Y. Lee et al., 2023; Wu et al., 2021). Interestingly, the OA from the three different biomass types group very distinctly in the H:C and O:C space as seen in Figure 4a. Especially, the savannah grass emissions are separated from the other two biomass types by their higher O:C ratio. The savannah grass O:C ratio is also high when compared with North American grass fire emissions, where O:C ratios ranging from 0.2 to 0.4 have been observed (Fortner et al., 2018). We do not observe effects from combustion conditions (i.e., MCE) on the H:C and O:C ratios (Figure S3a in Supporting Information S1), which is similar to previous open BB studies (J. Y. Lee et al., 2023), but in contrast with the strong MCE-dependency observed for residential wood combustion appliance emissions (Heringa et al., 2012).

The slope of H:C versus O:C for both boreal forest surface and savannah wood is close to −1 (−1.1 ± 0.1; Figure 4a), indicating that O:C ratio in POA is primarily driven by simultaneous changes in carbonyl and alcohol moieties (such as carboxylic group, COOH; Ng et al., 2011) for these biomasses. In contrast, the slope for savannah grass is shallower with a value of −0.7 ± 0.2. The shallower slope indicates that the O:C ratio in savannah grass POA is connected to a larger fraction of OH/OOH functional groups than for the two other biomasses, or COOH group addition to the site of a C-C bond cleavage (Ng et al., 2011) during POA formation.

For the three commonly used fractional AMS signals f_{43}, f_{44} and f_{60}, we find a similar, although not as distinctive, grouping by biomass as in the H:C and O:C space (Figures 4b and 4c). Generally, f_{43} is considered indicative of fresh OA, while f_{44} is attributed to oxygenated organic compounds and f_{60} is an indicator of levoglucosan-like compounds (Alfarra et al., 2007; Schneider et al., 2006). Using the HR-AMS data, we used CO_2^+ ion for f_{44} and $C_2H_4O_2^+$ ion for f_{60}. For the f_{43}, both $C_2H_3O^+$ and $C_3H_7^+$ ions would be observed at m/z 43 at unit mass resolution and for comparison with previous observations, we use the sum of these ions to calculate f_{43} in Figure 4b. In general, the POA data fall on the left edge of f_{43}-f_{44} triangle range in Figure 4b, which is typically occupied by ambient observations. Compared to the other two fuels, the higher f_{43} and lower f_{44} for the boreal forest surface indicate the higher faction of hydrocarbon fragments contained in the boreal forest surface POA (Figure 4b), which is further confirmed by the observed higher f_{C3H7} (Fig. S3b in Supporting Information S1). We also observe increased contribution from the $C_2H_3O^+$ ion for savannah grass (Figure S3b in Supporting Information S1), which can be attributed to the contribution of non-acid oxygenates. The observation is consistent with a shallower slope in the Van Krevelen diagram and a higher O:C ratio for savannah grass in Figure 4a. f_{43} has also been considered as an indicator of the H:C ratio (Ng et al., 2011). In Figure S3c in Supporting Information S1, we observe the highest correlation ($r = 0.96$) for H:C and f_{43}, when f_{43} is estimated as the sum of $C_2H_3O^+$ and $C_3H_7^+$ ions. Overall, BASFAA f_{43}, f_{44} and f_{60} are quite close to previous observations from laboratory campaigns using North American biomass (Ahern et al., 2019; Hennigan et al., 2011) and aircraft observations in savannah fire plumes by Wu et al. (2021).

We further looked into the composition of POA in the chamber using Positive Matrix Factorization (PMF) analysis. All experiments (primary emission phase, light and dark aging phase) were combined into a data set for each biomass type assessed in this study for PMF analysis. A 6-factor solution was chosen for the savannah wood and boreal forest surface data sets, and a 5-factor solution was chosen for the savannah grass. A detailed interpretation of all these factors will be presented in an upcoming paper. Here we focus on the composition of the primary particles. The factors were combined into 3 categories (Figure S4 in Supporting Information S1): a hydrocarbon-like OA factor with strong signal intensities for C_xH_y ions, a biomass-burning OA factor with prominent signals at levoglucosan related fragments ($C_2H_4O_2^+$ and $C_3H_5O_2^+$), and an oxygenated-primary OA factor with pronounced signals at $C_xH_yO_z$ ions (especially CO_2^+). Surprisingly, the biomass-burning OA factor often only forms a minor fraction of the primary OA (Figure S5 in Supporting Information S1), especially, for the boreal forest surface for which only 17% of OA is assigned to the biomass-burning OA factor on average. For the savannah biomasses, the biomass-burning OA factor contribution is larger, that is, on average 36% for savannah wood and 51% for savannah grass, respectively. However, some previous studies have also observed that all OA components generated from BB may not be assigned as a single conventional BBOA factor by PMF (Kortelainen et al., 2015; Tiitta et al., 2016). Unlike for the biomass type (Figure S5 in Supporting Information S1), we do not observe any systematic changes in the PMF factor contributions as a function of MCE.

Given the differences in the AMS OA composition for the different biomass types, we compared the novel SPMS composition for three different biomass-type experiments at similar MCE. In order to analyze the variance in the aerosol composition on a single-particle level, an exploratory principal component analysis was performed on the mass spectra from laser desorption/ionization for the different biomass types, see Figure S6 in Supporting Information S1. Principal Component Analysis identifies patterns in a set of (single-particle) mass spectra by reducing the data to a few main components that explain most of the variance. Each mass-to-charge ratio (m/z) is treated as a variable, and each single-particle spectrum as an observation. PCA finds combinations of m/z values (principal components) that best represent the differences between spectra. The SPMS-derived OC composition of the aerosols is quite similar, both for different fuels and between individual particles within each biomass type. This is reflected by the short eigenvectors of OC fragments of both polarities at the center of the plot (which are not annotated). However, the biomass types are separated by their inorganic composition, with the highest potassium signals determined for savannah wood, and stronger sulfate signatures detected for boreal forest surface and savannah grass. Negative carbon clusters are more prominent in savannah wood, while positive carbon

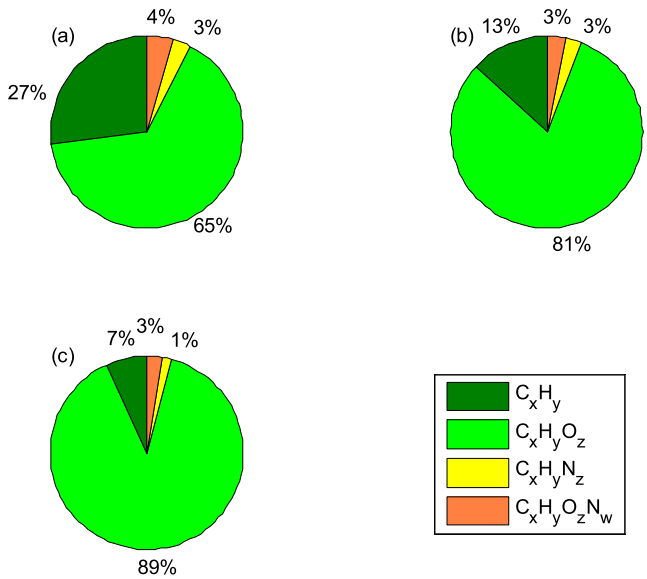

Figure 5. The average distribution of volatile organic compounds from Vocus measurements into hydrocarbons, oxygenated compounds and nitrogen containing compounds for primary emissions in (a) boreal forest surface, (b) savannah wood and (c) savannah grass experiments.

clusters dominate the EC signals in savannah grass particles. Nitrogen-containing compounds are more frequently detected in woody materials compared to the savannah grass smoke, but in different compositions. In SPMS, CN^- ions are associated with organonitrogen species in biomass combustion products, while the presence of NO_2^- and NO_3^- is more surprising, as they are typically attributed to secondary nitrate (Gunsch et al., 2018). The single-particle signatures of PAHs will be explored in a follow-up paper.

3.2.2. Volatile Organic Compounds

Similar characteristics appear as for the OA elemental ratios when investigating the composition of the VOC emissions measured by the Vocus spectrometer. Oxygenated compounds form the majority of VOC EFs (Figure 5) for all three biomasses, which is in line with previous observations (Koss et al., 2018). However, the relative contribution from hydrocarbons and oxygenated compounds changes from biomass to biomass. Specifically, boreal forest surface emissions have the largest hydrocarbon fraction of 27% of VOC EFs on average, whereas savannah wood (13%) and savannah grass (7%) have much lower hydrocarbon fractions (Figure 5). It should be kept in mind, though, that the Vocus does not detect all VOCs emitted by BB; for instance, small hydrocarbons such as methane and ethane are not detected. For all biomasses, nitrogen-containing compounds are observed, but they form only a small minority of the total VOC EFs.

Considering the distribution of VOCs in Figure 6, the C_5O_2 group of compounds is the largest contributor to the sum of Vocus-detected VOC EFs for all three biomasses. However, a clear difference between the boreal forest surface and the two savannah biomasses is the relatively high contribution from non-oxygenated C_{15}-ions (ions $C_{15}H_{23}$ and $C_{15}H_{25}$) to the boreal forest surface VOC emissions. Also, the savannah biomasses have a higher contribution from 2 to 4 carbon atom compounds compared to the boreal forest surface.

Previously, high- and low-temperature pyrolysis emission profiles have been identified in BB VOC emissions (Sekimoto et al., 2018). In our case, the limited number of observations at different MCEs does not allow for PMF analysis of the primary VOCs. Using a similar grouping of the data as in Figures 5 and 6, we find only minor effects from MCE (Figures S5 and S6 in Supporting Information S1). For savannah wood and -grass experiments, the fraction of C_5O_2 compounds increased slightly with decreasing MCE. For savannah grass, the glowing phase VOC emission is closer to that of the flaming than smoldering emissions in the O to C space (Figure S8 in Supporting Information S1). However, the changes are very small, which is qualitatively similar to a recent flight campaign in the US (Permar et al., 2021). A more detailed analysis of the VOCs observed in BASFAA experiments is in preparation.

3.3. Aerosol Particle Physical Properties

3.3.1. Size Distributions

The primary submicron aerosol particle size distribution appears to be affected more by combustion characteristics than by the type of biomass being burned (Figure 7). Especially, size distributions from the two savannah biomasses are comparable at similar MCEs. With increasing smoldering fraction, that is, decreasing MCE, the peak in the size distribution shifts toward larger sizes, exceeding 100 nm for the most smoldering experiments (Figure 7c). In the case of flaming combustion (Figure 7a), the size distribution peak shifts to smaller sizes at approximately 50 nm, similar to the observations by McClure et al. (2020). In most cases, the submicron size distribution is not unimodal. In Table S2 in Supporting Information S1, parameters for 2-modal log-normal fits are given for the size distributions in Figure 7. This is important to note especially when converting mass emissions into number size distribution (which is the case in most modeling studies), as the total mass is particularly sensitive to the large particles in the distribution.

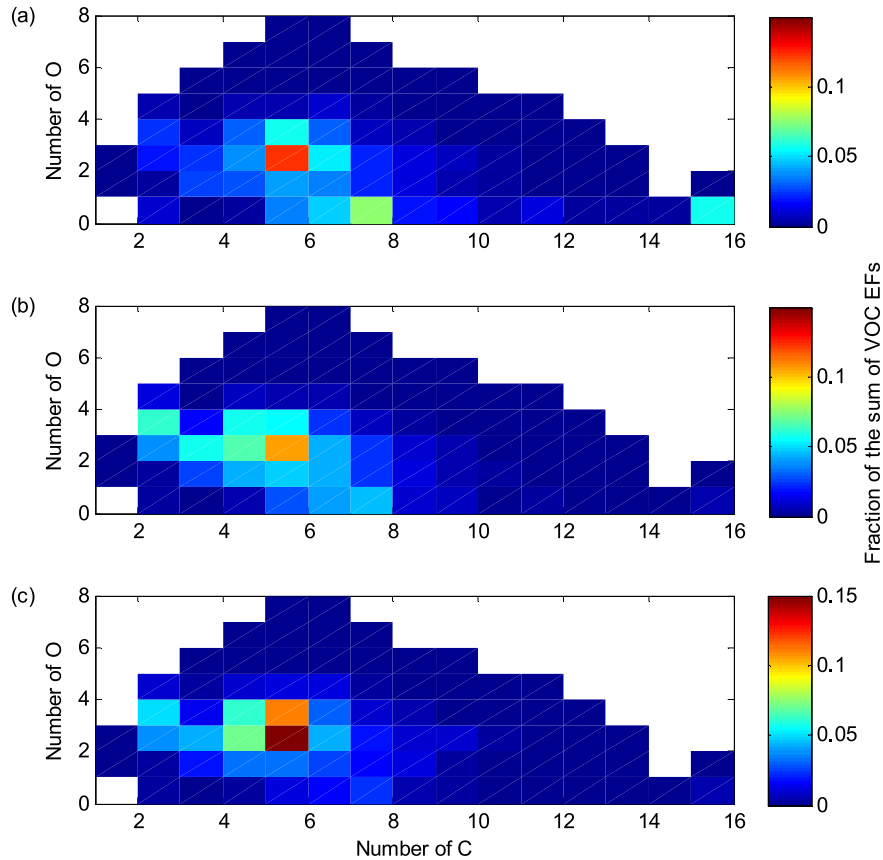

Figure 6. The fraction of total volatile organic compound EFs at a given number of O and C atoms for (a) boreal forest surface, (b) savannah wood and (c) savannah grass.

Compared with three previously used size distributions of open BB aerosol particles (Dentener et al., 2006; Stier et al., 2005; Vakkari et al., 2018), our study indicates considerable differences. Two of the literature size distributions (Dentener et al., 2006; Stier et al., 2005) are uni-modal, while the size distribution based on observations at the Welgegund research station in South Africa (Vakkari et al., 2018) is 3-modal. The Welgegund size distribution is based on fresh grassland and savannah fire smoke (age < 0.5 hr) and represents flaming-dominant

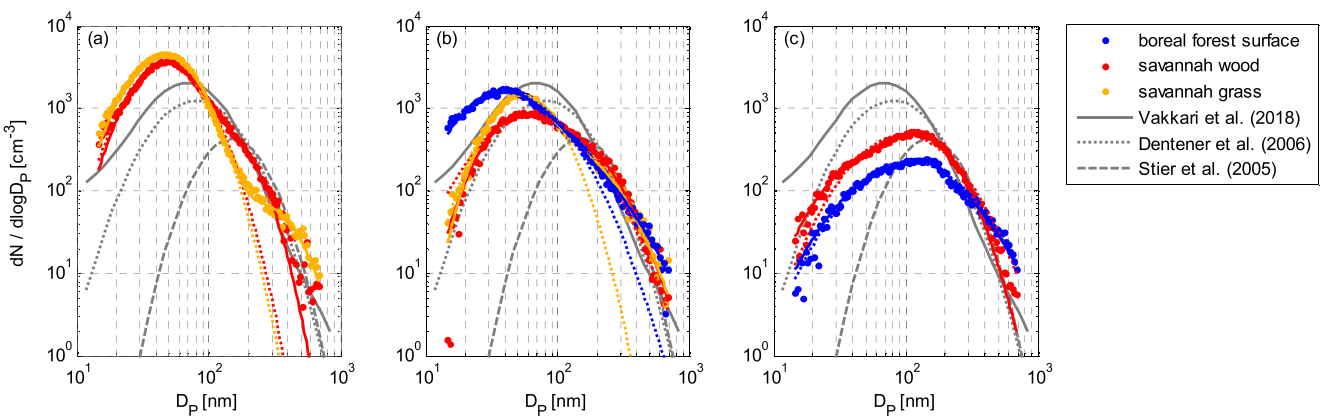

Figure 7. The median primary size distributions from SMPS measurements at three modified combustion efficiency (MCE) ranges for the three biomasses. Bimodal log-normal size distribution fits are indicated for the BASFAA experiments with solid lines. Unimodal fits are indicated with dashed lines. All size distributions were scaled to 1 μg m^{-3} mass concentration using a density of 1 g cm^{-3}. (a) Flaming emissions with MCE ranging from 0.94 to 0.96. (b) smoldering-dominated emissions with MCE ranging from 0.83 to 0.86. (c) Extreme smoldering emissions with MCE < 0.75.

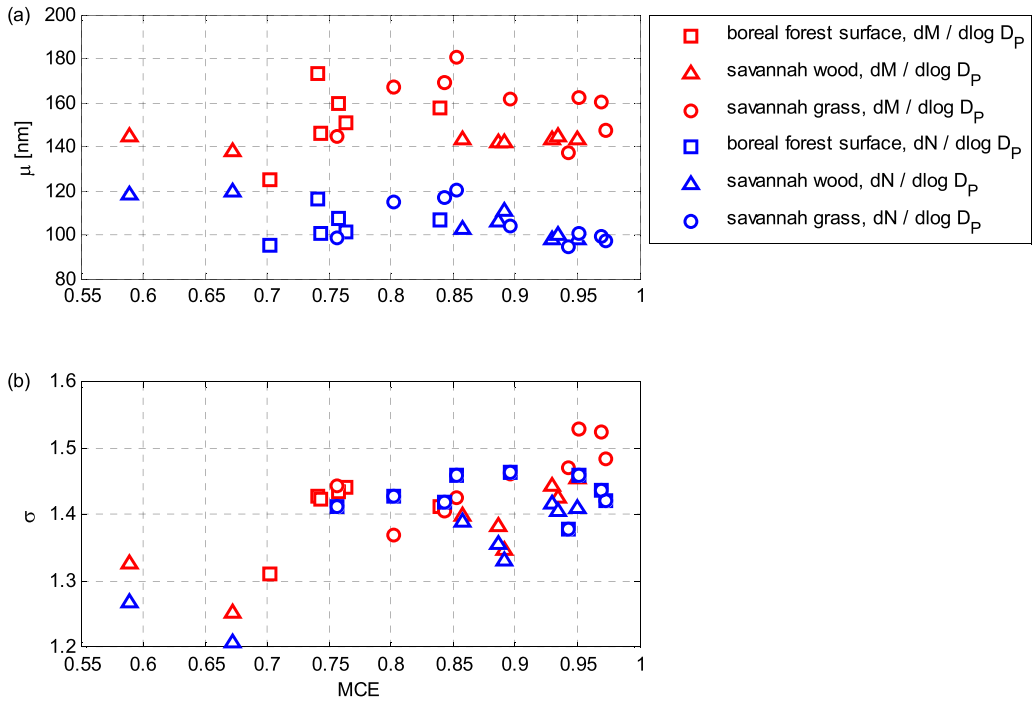

Figure 8. Unimodal log-normal fitting parameters for rBC mass and number size distributions from SP2 measurements as function of modified combustion efficiency. (a) Modal mean diameter. (b) Standard deviation of the log-normal mode.

emissions at an average MCE of 0.93 (Vakkari et al., 2018). However, the peak of the Welgegund distribution is larger than the chamber observations during the BASFAA campaign, which can be due to coagulation and condensational growth in the plume before it is dispersed into the boundary layer and observed at Welgegund. Overall, Figure 7 suggests that one should consider not only the age of the aerosol but also the combustion phase of the fire in choosing a representative size distribution when converting mass emissions into number size distribution.

Compared to the number size distribution, the rBC size distribution measured by the SP2 has much less variation, as seen in Figure 8. The fitted modal peak diameter is marginally smaller for high-MCE experiments for the rBC number size distribution. However, no such effect is seen for the rBC mass size distribution and the differences between the different biomasses are likewise very minor. Also, the average mass size distributions are readily described with one log-normal mode (Figure S9 in Supporting Information S1). The rBC mass size distributions peaking at approximately 150 nm are in good agreement with previous laboratory experiments on open BB (McClure et al., 2020), but smaller than what has been observed in fresh smoke in West Africa (Wu et al., 2021). The larger diameter of fresh atmospheric rBC is probably due to increased coagulation compared to laboratory experiments, as it is difficult to sample smoke younger than 15–30 min from an aircraft (e.g., Wu et al., 2021). Previously, both fresh and aged savannah fire rBC mass size distributions have been reported to peak in the range of 200–230 nm (Holanda et al., 2020, 2023; Taylor et al., 2020; Wu et al., 2021).

3.3.2. Aerosol Particle Density

PM1 mass emissions inferred from size distribution measurements (e.g., Vakkari et al., 2018) depend on the density of the particles and, especially, in the case of BB emissions, on the OA density, which has substantial uncertainty. Here, primary aerosol particle effective density was measured using a combination of APM and SMPS. On average (mean ± standard deviation), the effective density was 1.37 ± 0.04 g cm^{-3} for boreal forest surface emissions and 1.37 ± 0.09 g cm^{-3} for savannah wood emissions. For savannah grass experiments, we observed a slightly higher average effective density of 1.6 ± 0.1 g cm^{-3}. Overall, these are reasonably close to the previous chemical composition-based estimate of 1.485 ± 0.16 g cm^{-3} in Vakkari et al. (2018).

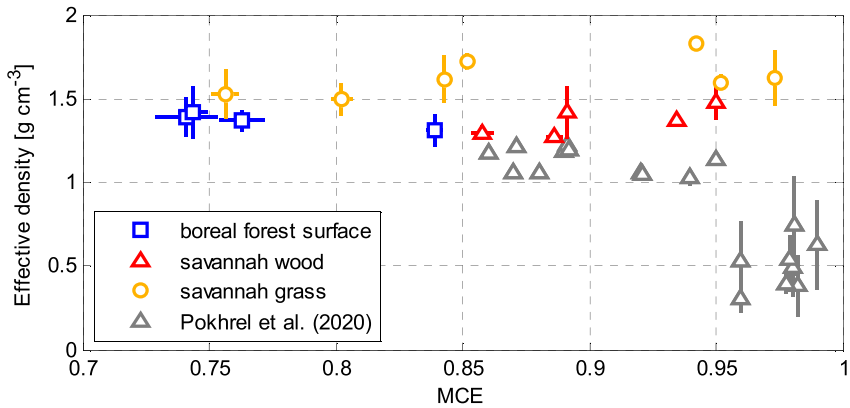

Figure 9. Measured effective density as a function of modified combustion efficiency (MCE). Values are averaged over all sizes, where effective density was measured. Error bars indicate the standard deviation for effective density and measurement uncertainty for MCE. Error bars that are not visible are smaller than the size of the marker.

Compared to laboratory experiments using six woody plant species from sub-Saharan Africa by Pokhrel et al. (2020), the effective density values in this study are distinctly higher (Figure 9). Furthermore, we found no dependency on MCE (Figure 9), in contrast to Pokhrel et al. (2020). Also contrary to Pokhrel et al. (2020), we found no size-dependency in the effective density even in the regime of MCE >0.95. This is probably related to the relatively low BC emissions from savannah grass flaming combustion in our experiments, which results in a lower fraction of non-spherical particles. One more difference between the studies is that the combustion setup in Pokhrel et al. (2020) was a tube furnace, whose temperature was controlled. This may have led to higher BC emission or more fractal structure of the BC cores than what would occur in open burning. We are not aware of effective density measurements from fresh savannah fire emissions in the field, and therefore cannot compare the effective densities with atmospheric observations. On the other hand, the very high OA fraction in our experiments, on average 95% (Figure 3), means that the effective density in Figure 9 is dominated by OA density. Using the chemical composition (Figure 3) and a similar calculation as in Vakkari et al. (2018), we estimated the OA density from the effective density in Figure 9. The mean (±standard deviation) OA density estimates are 1.37 ± 0.05 g cm^{-3} for boreal forest surface emissions, 1.34 ± 0.08 g cm^{-3} for savannah wood emissions and 1.6 ± 0.1 g cm^{-3} for savannah grass emissions. The higher density of savannah grass OA may reflect the higher O:C ratio (Figure 4).

3.3.3. Volatility Distributions

Average volatility distributions from the FIGAERO thermograms indicate rather similar volatility for the BASFAA particulates (Figure 10a). For boreal forest surface, the peak of the volatility distribution is clearly in the C* 10^0 μg m^{-3} bin, while for the two savannah biomasses the bulk of the aerosol is spread across the 10^{-1} μg m^{-3} and 10^0 μg m^{-3} bins, indicating higher fraction of compounds in the LVOC range (low-volatility organic compounds, C* < 3×10^{-1} μg m^{-3}). The fraction of aerosol with C* = 10^{-2} μg m^{-3} or less is quite similar for the three biomasses: 15% for boreal forest surface, 18% for savannah wood and 12% for savannah grass. For all three biomasses, the FIGAERO measurements thus indicate largely semi-volatile primary aerosol, which is in line with previous observations (e.g., May et al., 2013; Sinha et al., 2023).

We estimated the volatility distributions for the gas phase from the Vocus measurements using the parameterization of Li et al. (2016). Despite the differences observed in the chemical composition (Figures 5 and 6), the volatility distributions are very similar for all three biomasses (Figure 10b). Furthermore, we did not find any systematic effect of MCE on the volatility distributions, neither in particle phase data from FIGAERO (Figure S10 in Supporting Information S1) nor in gas phase data from Vocus (Figure S11 in Supporting Information S1). However, a relatively low OA/rBC ratio appears to be related to lower particle phase volatility for savannah grass emissions (Figure S12 in Supporting Information S1), which is similar to McClure et al. (2020). We did not, however, find any effect from the OA/rBC ratio for other biomasses or gas phase volatility distributions (Figures S12 and S13 in Supporting Information S1).

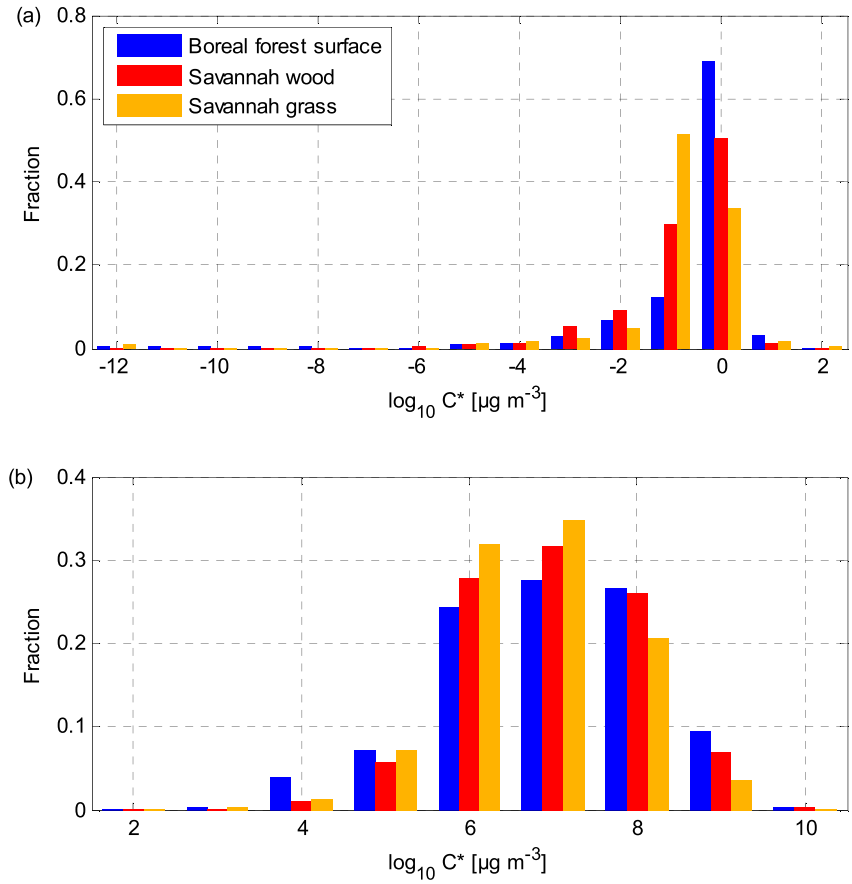

Figure 10. Mean volatility distributions for the three biomasses, grouped into decadal bins of effective saturation vapor concentrations (C*). (a) Particle phase from FIGAERO measurements. (b) Gas phase from Vocus measurements.

3.3.4. Optical Properties

Plotting SSA as a function of MCE, we observe a decrease in the SSA for flaming-dominated combustion (Figure 11a). This is a well-known feature (e.g., Liu et al., 2014) and related to non-linear BC formation with high MCE. However, for MCE > 0.90, the SSA values we find are higher than those presented by Liu et al. (2014) and also higher than SSA values reported previously for savannah and grassland fires (e.g., Brown et al., 2021; Vakkari et al., 2014). This is evidently due to lower BC formation in our setup than in landscape scale savannah fires, as discussed earlier, and therefore we do not recommend using the flaming-dominated (MCE > 0.90) SSA values from our study. On the other hand, for the smoldering dominated emissions (MCE < 0.90) the SSA values reported here agree reasonably well with previous observations for relatively low BC content smoke, where SSA approaches 0.97 at both 550 and 700 nm wavelengths (Brown et al., 2021). For smoldering-dominated combustion, we observe a distinct decrease in SSA with decreasing wavelength (Figure 11b), which we attribute to increasing contribution of BrC absorption in the shorter wavelengths. Similar spectral dependency is also present in our flaming-dominated SSA data. On average, smoldering-dominated SSA is a little higher for boreal forest surface than for the two savannah biomasses, but the difference is small (Figure 11b).

The effect of BrC is clearly visible in the AAE (Figure 12), with a mean (± standard deviation) of 2.6 (±0.6) for wavelengths 370–950 nm. Compared to North American biomass (Selimovic et al., 2018), we observe a less steep increase in AAE with decreasing MCE in Figure 12a. For the North American biomass, the AAE calculated for 401 and 807 nm was >7.2 at MCE of 0.80; at MCE of 0.95, the AAE was 1.96 in Selimovic et al. (2018). However, in our experiments, AAE is not constant over the full wavelength range. For the shorter wavelengths (370–520 nm), AAE is substantially larger, on average 3.9 (±0.9), than for the longer wavelengths (520–950 nm), where the average AAE is 2.1 (±0.7). Thus, the potential wavelength dependency of the AAE should be kept in mind when interpreting absorption spectra (c.f. Zotter et al., 2017).

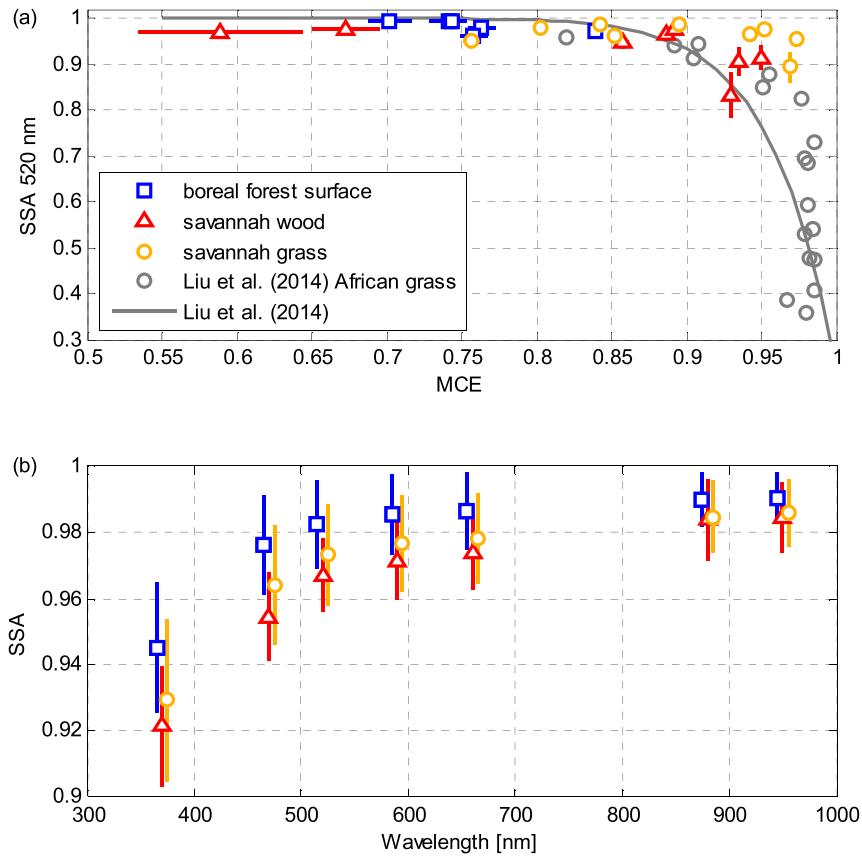

Figure 11. (a) single scattering albedo (SSA) at 520 nm as a function of modified combustion efficiency (MCE). Error bars indicate measurement uncertainty. Laboratory burn data for African grass and fit at 532 nm from Liu et al. (2014) are included. Note that the fit is not only for grass but also for all biomasses included in Liu et al. (2014). Also note that the four savannah grass experiments at MCE > 0.90 are affected by reduced black carbon formation in our experiments. (b) Mean SSA for smoldering experiments (MCE < 0.90) as a function of wavelength. Error bars indicate standard deviation. Error bars that are not visible are smaller than the size of the marker.

Recently, McClure et al. (2020) showed that many optical properties of BB aerosols depend more on the OA/BC ratio than MCE, which is also seen for AAE in our experiments (Figure 12b). Especially, the short wavelength AAE (370–520 nm) increases strongly with increasing OA/rBC, which is similar to McClure et al. (2020). On the other hand, the biomass type does not appear to have any effect on the AAE, but all three studied biomasses follow on the same trend in Figure 12b.

In a recent aircraft campaign, Wu et al. (2021) observed relatively low AAE for savannah fire aerosols, in the order of 1–1.9, increasing with the age of the smoke. In comparison to the OA/rBC range in Figure 12b, the smoke layers sampled by Wu et al. (2021) had a relatively low OA/BC ratio (5–10, approximately). Also, in Wu et al. (2021) the AAE was determined using 658 nm as the longer wavelength, which in our case results in lower AAE than that determined at wavelengths shorter than 520 nm. With these considerations, the AAE observed by Wu et al. (2021) is actually relatively close to our lowest OA/rBC savannah wood data point in Figure 12b.

For MAC_{rBC} (Figure S14 in Supporting Information S1) we find similar dependency on OA/rBC ratio than McClure et al. (2020), with extremely high MAC_{rBC} at high OA/rBC. In Figure S14 in Supporting Information S1, the observed MAC_{rBC} is compared with the commonly used uncoated MAC_{BC} value of 7.5 ± 1.2 m^2 g^{-1} at 550 nm wavelength (Bond & Bergstrom, 2006), which is extrapolated to other wavelengths with a-used AAE of 1.0 (Bond et al., 2013; Zotter et al., 2017). However, AAE of BC depends on microphysical properties such as core size, internal structure and coating (Gyawali et al., 2009; Luo et al., 2023; Virkkula, 2021) and considering the rBC size distributions (Figure 8) we include an uncertainty of ±0.2 in the BC AAE for MAC_{BC} in Figure S14 in Supporting Information S1. At short wavelengths, the observed MAC_{rBC} is greater than the reference MAC_{BC}

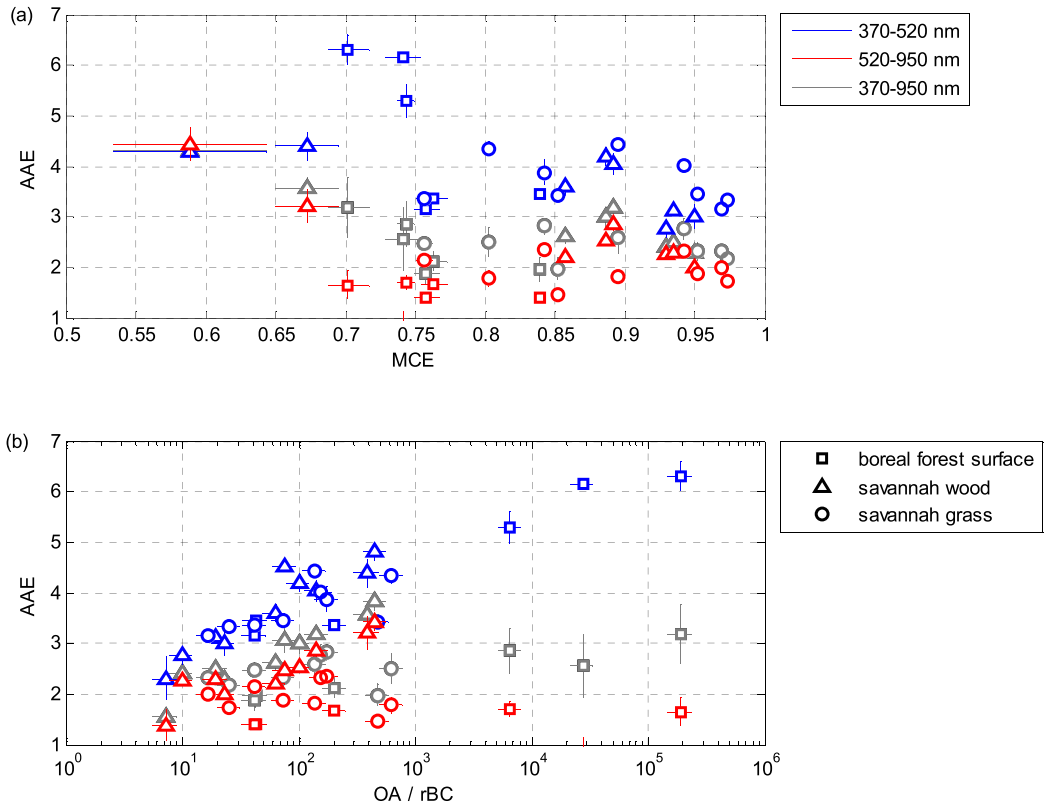

Figure 12. (a) Absorption Ångström exponent (AAE) at three wavelength ranges as function of modified combustion efficiency (MCE). AAE is derived from a least squares fit and error bars indicate standard error of the fit. For MCE, error bars indicate measurement uncertainty. Error bars that are not visible are smaller than the size of the marker. (b) Same as in (a), but as a function of the organic aerosol/rBC ratio. Biomass type is indicated in both panels with the markers indicated in (b) and AAE wavelength range with color indicated in (a).

even at the lowest OA/rBC ratios that we observed, which is another indication of absorption by BrC. At longest wavelengths (880 and 950 nm) some of the experiments with the lowest OA/rBC ratio indicate even lower MAC_{rBC} than the reference value from Bond and Bergstrom (2006). However, the difference is within the measurement uncertainty.

At very high OA/rBC (>1,000), the observed MAC_{rBC} (Figure S14 in Supporting Information S1) is extremely high even at the longest wavelengths. For comparison, we used Mie calculations to model MAC_{rBC} using rBC size distributions from Figure 8, observed OA/rBC ratio and assuming internally mixed aerosol with non-absorbing coating material. The calculations were performed using the same code as in Virkkula (2021). This is an extreme upper limit case for modeling MAC_{rBC}, as only a minimal fraction of particles contains rBC in high OA/rBC cases (Figure S15 in Supporting Information S1). We note that also in atmospheric observations of fresh BB plumes, external mixture with rBC is typical (e.g., Wu et al., 2021). Even with the internally mixed assumption, the observed MAC_{rBC} cannot be explained solely by absorption enhancement through non-absorbing coating (Figure S14 in Supporting Information S1).

We estimate the upper limit of OA mass absorption coefficient (MAC_{OA}) assuming no mixing-induced absorption enhancement and using the uncoated BC reference value from Bond and Bergstrom (2006) with uncertainties as in Fig. S14 in Supporting Information S1 (see Text S2 in Supporting Information S1). At short wavelengths, MAC_{OA} (Figure S16 in Supporting Information S1) increases with decreasing OA/rBC ratio, similar to McClure et al. (2020). Previously, this dependency has been attributed to primary BrC becoming darker as combustion conditions approach the regime of BC formation (McClure et al., 2020; Saleh et al., 2018). At longer wavelengths, the low OA/rBC range MAC_{OA} is highly uncertain due to the uncertainties in the MAC_{rBC}. However, at high OA/rBC (>300) we find MAC_{OA} consistently greater than 0 at all wavelengths (Figure S16 in

Table 3
Average (±Standard Deviation) MAC_{OA} for High OA/rBC Experiments (OA/rBC > 300)

	MAC_{OA} [m^2 g^{-1}]		
Wavelength [nm]	Boreal forest surface N = 3, MCE = 0.73	Savannah wood N = 2, MCE = 0.67	Savannah grass N = 2, MCE = 0.83
370	0.47 ± 0.05	0.82 ± 0.03	0.69 ± 0.02
470	0.12 ± 0.02	0.28 ± 0.03	0.27 ± 0.02
520	0.062 ± 0.01	0.15 ± 0.02	0.18 ± 0.02
590	0.043 ± 0.008	0.097 ± 0.01	0.15 ± 0.03
660	0.036 ± 0.005	0.071 ± 0.01	0.13 ± 0.02
880	0.025 ± 0.003	0.015 ± 0.002	0.076 ± 0.02
950	0.025 ± 0.002	0.017 ± 0.005	0.065 ± 0.02

Note. Number of experiments (N) and average MCE is also indicated. For savannah wood, MCE is available for only one of the two experiments.

Supporting Information S1), as shown also in Table 3. The MAC_{OA} values in Table 3 are reasonably close to the values of 0.76, 0.21 and 0.056 m^2 g^{-1} at 405, 532 and 781 nm, respectively, reported by McClure et al. (2020).

4. Conclusions

We performed a series of laboratory experiments to characterize the primary emissions from open burning and their variability with combustion conditions for three different biomasses, that is, boreal forest surface, savannah grass and savannah wood. The BASFAA experiments in this study offer the most comprehensive characterization of open burning emissions to date for southern African savannah biomasses. For the European boreal forest, this is the first time that primary emissions from surface layer fires have been characterized, although in the European boreal forest fires often only consume the surface layer.

EF of OA and VOCs are largely dependent on combustion characteristics quantified through MCE, which is well in line with previous observations. Our experiments show that the linear relationships between MCE and EF_{OA}, as well as between MCE and the sum of EF_{VOC}, extend to as low MCE as 0.6. This indicates that even a relatively small amount of biomass consumed in extreme smoldering conditions can emit substantial amounts of OA and VOCs. Interestingly, EF_{OA} and the sum of EF_{VOC} appear to have a relatively similar trend with MCE for all three types of biomass considered in our experiments. However, MCE cannot distinguish the glowing phase of fire after flames have died down, from smoldering combustion. This has a major effect on the EFs, which are naturally much lower for the glowing phase. Notably, the aerosol particle size distribution also depends on MCE, with the size distribution being described with a bimodal log-normal size distribution, which should be observed, especially, when converting mass emissions into a number size distribution.

Optical properties are strongly affected by BC formation, which is not surprising. However, the optical properties of OA depend more on the OA/rBC ratio than on MCE, which further indicates that MCE is not sufficient to characterize all relevant aspects of the combustion process. Our measurements also indicate non-zero, albeit low, MAC_{OA}, even for the longest wavelengths of 880 and 950 nm. This is noteworthy, as in analysis of multi-wavelength absorption spectra it is frequently assumed that absorption at these wavelengths is only due to BC. In our case of fresh open BB emissions, such an assumption would result in overestimation of BC contribution to aerosol absorption. AAE and MAC_{OA}, however, are among the parameters where biomass type has minimal effect compared to combustion process.

Despite similarities in the EFs and some other parameters, biomass type does have a substantial effect on the composition of OA and VOCs. Considering OA, we find distinct grouping by biomass type in the Van Krevelen diagram with the largest O:C for savannah grass. Thus, in fresh smoke, small changes in the O:C ratio may be due to changes in burned biomass composition in addition to atmospheric oxidation, which need to be kept in mind when analyzing atmospheric evolution of OA in savannah fire plumes. Similarly, the fraction of oxygenated VOCs is much higher for savannah grass compared to the two other biomass types, which have lower O:C ratio also in the particle phase OA.

Overall, our observations offer parameterizations for OA and VOC emissions as a function of MCE from two relatively understudied biomes. For European boreal forest, the EFs we provide enable for the first differentiation between crown and surface fires in emission inventories and modeling studies. Similarly, the EFs for savannah grass enable differentiating grasslands from savannahs in emission inventories and the MCE-dependency of EFs can be used to further adjust the emissions based on combustion conditions. The characterization of the primary emissions also provides a starting point for analyzing the aging of the African savannah and European boreal forest fire emissions, both in laboratory experiments and in the atmosphere.

Conflict of Interest

The authors declare no conflicts of interest relevant to this study.

Availability Statement

The BASFAA data used in the study are available at METIS - FMI's Research Data repository via http://doi.org/10.57707/fmi-b2share.16d432b62932448fbbf5ca38aaaef603 with CC-BY license (Vakkari et al., 2025).

Acknowledgments
This project was supported by the Research Council of Finland (Grants 337550, 343359, 341597, 346371, 364229, 374081, 374082) and by the European Commission under the Horizon 2020–Research and Innovation Framework Programme, H2020-INFRAIA-2020-1, Grant Agreement number: 101008004. Funding from the Helmholtz association in the framework of the "aeroHEALTH" Helmholtz International Lab is gratefully acknowledged.

References

Aakala, T., Pasanen, L., Helama, S., Vakkari, V., Drobyshev, I., Seppä, H., et al. (2017). Multiscale variation in drought controlled historical forest fire activity in the boreal forests of eastern Fennoscandia. *Ecological Monographs*, *88*(1), 74–91. https://doi.org/10.1002/ecm.1276

Abatzoglou, J. T., Battisti, D. S., Williams, A. P., Hansen, W. D., Harvey, B. J., & Kolden, C. A. (2021). Projected increases in western US forest fire despite growing fuel constraints. *Communications Earth & Environment*, *2*(1), 227. https://doi.org/10.1038/s43247-021-00299-0

Abatzoglou, J. T., Williams, A. P., & Barbero, R. (2019). Global emergence of anthropogenic climate change in fire weather indices. *Geophysical Research Letters*, *46*(1), 326–336. https://doi.org/10.1029/2018GL080959

Ahern, A. T., Robinson, E. S., Tkacik, D. S., Saleh, R., Hatch, L. E., Barsanti, K. C., et al. (2019). Production of secondary organic aerosol during aging of biomass burning smoke from fresh fuels and its relationship to VOC precursors. *Journal of Geophysical Research: Atmospheres*, *124*(6), 3583–3606. https://doi.org/10.1029/2018JD029068

Akagi, S. K., Yokelson, R. J., Wiedinmyer, C., Alvarado, M. J., Reid, J. S., Karl, T., et al. (2011). Emission factors for open and domestic biomass burning for use in atmospheric models. *Atmospheric Chemistry and Physics*, *11*(9), 4039–4072. https://doi.org/10.5194/acp-11-4039-2011

Alfarra, M. R., Prevot, A. S. H., Szidat, S., Sandradewi, J., Weimer, S., Lanz, V. A., et al. (2007). Identification of the mass spectral signature of organic aerosols from wood burning emissions. *Environmental Science & Technology*, *41*(16), 5770–5777. https://doi.org/10.1021/es062289b

Andreae, M. O. (2019). Emission of trace gases and aerosols from biomass burning–An updated assessment. *Atmospheric Chemistry and Physics*, *19*(13), 8523–8546. https://doi.org/10.5194/acp-19-8523-2019

Bannan, T. J., Le Breton, M., Priestley, M., Worrall, S. D., Bacak, A., Marsden, N. A., et al. (2019). A method for extracting calibrated volatility information from the FIGAERO-HR-ToF-CIMS and its experimental application. *Atmospheric Measurement Techniques*, *12*(3), 1429–1439. https://doi.org/10.5194/amt-12-1429-2019

Bertschi, I., Yokelson, R. J., Ward, D. E., Babbitt, R. E., Susott, R. A., Goode, J. G., & Hao, W. M. (2003). Trace gas and particle emissions from fires in large diameter and belowground biomass fuels. *Journal of Geophysical Research*, *108*(D13). https://doi.org/10.1029/2002JD002100

Binte Shahid, S., Lacey, F. G., Wiedinmyer, C., Yokelson, R. J., & Barsanti, K. C. (2024). NEIVAv1.0: Next-generation Emissions InVentory expansion of Akagi et al. (2011) version 1.0. *Geoscientific Model Development*, *17*(21), 7679–7711. https://doi.org/10.5194/gmd-17-7679-2024

Bond, T. C., & Bergstrom, R. W. (2006). Light absorption by carbonaceous particles: An investigative review. *Aerosol Science and Technology*, *40*(1), 27–67. https://doi.org/10.1080/02786820500421521

Bond, T. C., Doherty, S. J., Fahey, D. W., Forster, P. M., Berntsen, T., DeAngelo, B. J., et al. (2013). Bounding the role of black carbon in the climate system: A scientific assessment. *Journal of Geophysical Research: Atmospheres*, *118*(11), 5380–5552. https://doi.org/10.1002/jgrd.50171

Brown, H., Liu, X., Pokhrel, R., Murphy, S., Lu, Z., Saleh, R., et al. (2021). Biomass burning aerosols in most climate models are too absorbing. *Nature Communications*, *12*(1), 277. https://doi.org/10.1038/s41467-020-20482-9

Canagaratna, M. R., Jimenez, J. L., Kroll, J. H., Chen, Q., Kessler, S. H., Massoli, P., et al. (2015). Elemental ratio measurements of organic compounds using aerosol mass spectrometry: Characterization, improved calibration, and implications. *Atmospheric Chemistry and Physics*, *15*(1), 253–272. https://doi.org/10.5194/acp-15-253-2015

Cantrell, C. A. (2008). Technical Note: Review of methods for linear least-squares fitting of data and application to atmospheric chemistry problems. *Atmospheric Chemistry and Physics*, *8*(17), 5477–5487. https://doi.org/10.5194/acp-8-5477-2008

Capes, G., Johnson, B., McFiggans, G., Williams, P. I., Haywood, J., & Coe, H. (2008). Aging of biomass burning aerosols over West Africa: Aircraft measurements of chemical composition, microphysical properties, and emission ratios. *Journal of Geophysical Research*, *113*(D23). https://doi.org/10.1029/2008JD009845

Che, H., Segal-Rozenhaimer, M., Zhang, L., Dang, C., Zuidema, P., Dobracki, A., et al. (2022). Cloud processing and weeklong ageing affect biomass burning aerosol properties over the south-eastern Atlantic. *Communications Earth & Environment*, *3*(1), 182. https://doi.org/10.1038/s43247-022-00517-3

Chen, Q., Heald, C. L., Jimenez, J. L., Canagaratna, M. R., Zhang, Q., He, L.-Y., et al. (2015). Elemental composition of organic aerosol: The gap between ambient and laboratory measurements. *Geophysical Research Letters*, *42*(10), 4182–4189. https://doi.org/10.1002/2015GL063693

Christian, H. J., Blakeslee, R. J., Boccippio, D. J., Boeck, W. L., Buechler, D. E., Driscoll, K. T., et al. (2003). Global frequency and distribution of lightning as observed from space by the Optical Transient Detector. *Journal of Geophysical Research*, *108*(D1), 4005. https://doi.org/10.1029/2002JD002347

Christian, T. J., Kleiss, B., Yokelson, R. J., Holzinger, R., Crutzen, P. J., Hao, W. M., et al. (2004). Comprehensive laboratory measurements of biomass-burning emissions: 2. First intercomparison of open-path FTIR, PTR-MS, and GC-MS/FID/ECD. *Journal of Geophysical Research*, *109*(D2). https://doi.org/10.1029/2003JD003874

Collaud Coen, M., Weingartner, E., Apituley, A., Ceburnis, D., Fierz-Schmidhauser, R., Flentje, H., et al. (2010). Minimizing light absorption measurement artifacts of the aethalometer: Evaluation of five correction algorithms. *Atmospheric Measurement Techniques*, *3*(2), 457–474. https://doi.org/10.5194/amt-3-457-2010

Collier, S., Zhou, S., Onasch, T. B., Jaffe, D. A., Kleinman, L., Sedlacek, A. J., et al. (2016). Regional influence of aerosol emissions from wildfires driven by combustion efficiency: Insights from the BBOP campaign. *Environmental Science & Technology*, *50*(16), 8613–8622. https://doi.org/10.1021/acs.est.6b01617

DeCarlo, P. F., Kimmel, J. R., Trimborn, A., Northway, M. J., Jayne, J. T., Aiken, A. C., et al. (2006). Field-deployable, high-resolution, time-of-flight aerosol mass spectrometer. *Analytical Chemistry*, *78*(24), 8281–8289. https://doi.org/10.1021/ac061249n

Dentener, F., Kinne, S., Bond, T., Boucher, O., Cofala, J., Generoso, S., et al. (2006). Emissions of primary aerosol and precursor gases in the years 2000 and 1750 prescribed data-sets for AeroCom. *Atmospheric Chemistry and Physics*, *6*(12), 4321–4344. https://doi.org/10.5194/acp-6-4321-2006

Desservettaz, M., Paton-Walsh, C., Griffith, D. W. T., Kettlewell, G., Keywood, M. D., Vanderschoot, M. V., et al. (2017). Emission factors of trace gases and particles from tropical savanna fires in Australia. *Journal of Geophysical Research: Atmospheres*, *122*(11), 6074. https://doi.org/10.1002/2016JD025925

Dobracki, A., Zuidema, P., Howell, S. G., Saide, P., Freitag, S., Aiken, A. C., et al. (2023). An attribution of the low single-scattering albedo of biomass burning aerosol over the southeastern Atlantic. *Atmospheric Chemistry and Physics*, *23*(8), 4775–4799. https://doi.org/10.5194/acp-23-4775-2023

Docherty, K. S., Jaoui, M., Corse, E., Jimenez, J. L., Offenberg, J. H., Lewandowski, M., & Kleindienst, T. E. (2013). Collection efficiency of the aerosol mass spectrometer for chamber-generated secondary organic aerosols. *Aerosol Science and Technology*, *47*(3), 294–309. https://doi.org/10.1080/02786826.2012.752572

Fortner, E., Onasch, T., Canagaratna, M., Williams, L. R., Lee, T., Jayne, J., & Worsnop, D. (2018). Examining the chemical composition of black carbon particles from biomass burning with SP-AMS. *Journal of Aerosol Science*, *120*, 12–21. https://doi.org/10.1016/j.jaerosci.2018.03.001

Gkatzelis, G. I., Coggon, M. M., Stockwell, C. E., Hornbrook, R. S., Allen, H., Apel, E. C., et al. (2024). Parameterizations of US wildfire and prescribed fire emission ratios and emission factors based on FIREX-AQ aircraft measurements. *Atmospheric Chemistry and Physics*, *24*(2), 929–956. https://doi.org/10.5194/acp-24-929-2024

Gunsch, M. J., May, N. W., Wen, M., Bottenus, C. L. H., Gardner, D. J., VanReken, T. M., et al. (2018). Ubiquitous influence of wildfire emissions and secondary organic aerosol on summertime atmospheric aerosol in the forested Great Lakes region. *Atmospheric Chemistry and Physics*, *18*(5), 3701–3715. https://doi.org/10.5194/acp-18-3701-2018

Gyawali, M., Arnott, W. P., Lewis, K., & Moosmüller, H. (2009). In situ aerosol optics in Reno, NV, USA during and after the summer 2008 California wildfires and the influence of absorbing and non-absorbing organic coatings on spectral light absorption. *Atmospheric Chemistry and Physics*, *9*(20), 8007–8015. https://doi.org/10.5194/acp-9-8007-2009

Gysel, M., Laborde, M., Olfert, J. S., Subramanian, R., & Gröhn, A. J. (2011). Effective density of Aquadag and fullerene soot black carbon reference materials used for SP2 calibration. *Atmospheric Measurement Techniques*, *4*(12), 2851–2858. https://doi.org/10.5194/amt-4-2851-2011

Haslett, S. L., Taylor, J. W., Evans, M., Morris, E., Vogel, B., Dajuma, A., et al. (2019). Remote biomass burning dominates southern West African air pollution during the monsoon. *Atmospheric Chemistry and Physics*, *19*(24), 15217–15234. https://doi.org/10.5194/acp-19-15217-2019

Hennigan, C. J., Miracolo, M. A., Engelhart, G. J., May, A. A., Presto, A. A., Lee, T., et al. (2011). Chemical and physical transformations of organic aerosol from the photo-oxidation of open biomass burning emissions in an environmental chamber. *Atmospheric Chemistry and Physics*, *11*(15), 7669–7686. https://doi.org/10.5194/acp-11-7669-2011

Heringa, M. F., DeCarlo, P. F., Chirico, R., Lauber, A., Doberer, A., Good, J., et al. (2012). Time-resolved characterization of primary emissions from residential wood combustion appliances. *Environmental Science & Technology*, *46*(20), 11418–11425. https://doi.org/10.1021/es301654w

Hodshire, A. L., Akherati, A., Alvarado, M. J., Brown-Steiner, B., Jathar, S. H., Jimenez, J. L., et al. (2019). Aging effects on biomass burning aerosol mass and composition: A critical review of field and laboratory studies. *Environmental Science & Technology*, *53*(17), 10007–10022. https://doi.org/10.1021/acs.est.9b02588

Holanda, B. A., Franco, M. A., Walter, D., Artaxo, P., Carbone, S., Cheng, Y., et al. (2023). African biomass burning affects aerosol cycling over the Amazon. *Communications Earth & Environment*, *4*(1), 154. https://doi.org/10.1038/s43247-023-00795-5

Holanda, B. A., Pöhlker, M. L., Walter, D., Saturno, J., Sörgel, M., Ditas, J., et al. (2020). Influx of African biomass burning aerosol during the Amazonian dry season through layered transatlantic transport of black carbon-rich smoke. *Atmospheric Chemistry and Physics*, *20*(8), 4757–4785. https://doi.org/10.5194/acp-20-4757-2020

Jaars, K., van Zyl, P. G., Beukes, J. P., Hellén, H., Vakkari, V., Josipovic, M., et al. (2016). Measurements of biogenic volatile organic compounds at a grazed savannah grassland agricultural landscape in South Africa. *Atmospheric Chemistry and Physics*, *16*(24), 15665–15688. https://doi.org/10.5194/acp-16-15665-2016

Jaffe, D. A., O'Neill, S. M., Larkin, N. K., Holder, A. L., Peterson, D. L., Halofsky, J. E., & Rappold, A. G. (2020). Wildfire and prescribed burning impacts on air quality in the United States. *Journal of the Air & Waste Management Association*, *70*(6), 583–615. https://doi.org/10.1080/10962247.2020.1749731

Janhäll, S., Andreae, M. O., & Pöschl, U. (2010). Biomass burning aerosol emissions from vegetation fires: Particle number and mass emission factors and size distributions. *Atmospheric Chemistry and Physics*, *10*(3), 1427–1439. https://doi.org/10.5194/acp-10-1427-2010

Jen, C. N., Hatch, L. E., Selimovic, V., Yokelson, R. J., Weber, R., Fernandez, A. E., et al. (2019). Speciated and total emission factors of particulate organics from burning western US wildland fuels and their dependence on combustion efficiency. *Atmospheric Chemistry and Physics*, *19*(2), 1013–1026. https://doi.org/10.5194/acp-19-1013-2019

Jensen, A. R., Koss, A. R., Hales, R. B., & de Gouw, J. A. (2023). Measurements of volatile organic compounds in ambient air by gas-chromatography and real-time Vocus PTR-TOF-MS: Calibrations, instrument background corrections, and introducing a PTR data toolkit. *Atmospheric Measurement Techniques*, *16*(21), 5261–5285. https://doi.org/10.5194/amt-16-5261-2023

Jimenez, J. L., Canagaratna, M. R., Drewnick, F., Allan, J. D., Alfarra, M. R., Middlebrook, A. M., et al. (2016). Comment on "The effects of molecular weight and thermal decomposition on the sensitivity of a thermal desorption aerosol mass spectrometer". *Aerosol Science and Technology*, *50*(9), i–xv. https://doi.org/10.1080/02786826.2016.1205728

Jimenez, J. L., Jayne, J. T., Shi, Q., Kolb, C. E., Worsnop, D. R., Yourshaw, I., et al. (2003). Ambient aerosol sampling using the aerodyne aerosol mass spectrometer. *Journal of Geophysical Research*, *108*(D7). https://doi.org/10.1029/2001JD001213

Kommula, S. M., Buchholz, A., Gramlich, Y., Mielonen, T., Hao, L., Pullinen, I., et al. (2024). Effect of long-range transported fire aerosols on cloud condensation nuclei concentrations and cloud properties at high latitudes. *Geophysical Research Letters*, *51*(6), e2023GL107134. https://doi.org/10.1029/2023GL107134

Kortelainen, A., Joutsensaari, J., Hao, L., Leskinen, J., Tiitta, P., Jaatinen, A., et al. (2015). Real-time chemical composition analysis of particulate emissions from woodchip combustion. *Energy & Fuels*, *29*(2), 1143–1150. https://doi.org/10.1021/ef5019548

Koss, A. R., Sekimoto, K., Gilman, J. B., Selimovic, V., Coggon, M. M., Zarzana, K. J., et al. (2018). Non-methane organic gas emissions from biomass burning: Identification, quantification, and emission factors from PTR-ToF during the FIREX 2016 laboratory experiment. *Atmospheric Chemistry and Physics*, *18*(5), 3299–3319. https://doi.org/10.5194/acp-18-3299-2018

Köster, K., Kohli, J., Lindberg, H., & Pumpanen, J. (2024). Post-fire soil greenhouse gas fluxes in boreal Scots pine forests–Are they affected by surface fires with different severities? *Agricultural and Forest Meteorology*, *349*, 109954. https://doi.org/10.1016/j.agrformet.2024.109954

Krechmer, J., Lopez-Hilfiker, F., Koss, A., Hutterli, M., Stoermer, C., Deming, B., et al. (2018). Evaluation of a new reagent-ion source and focusing ion–molecule reactor for use in proton-transfer-reaction mass spectrometry. *Analytical Chemistry*, *90*(20), 12011–12018. https://doi.org/10.1021/acs.analchem.8b02641

Krieger, U. K., Siegrist, F., Marcolli, C., Emanuelsson, E. U., Gøbel, F. M., Bilde, M., et al. (2018). A reference data set for validating vapor pressure measurement techniques: Homologous series of polyethylene glycols. *Atmospheric Measurement Techniques*, *11*(1), 49–63. https://doi.org/10.5194/amt-11-49-2018

Lee, B. H., Lopez-Hilfiker, F. D., Mohr, C., Kurtén, T., Worsnop, D. R., & Thornton, J. A. (2014). An iodide-adduct high-resolution time-of-flight chemical-ionization mass spectrometer: Application to atmospheric inorganic and organic compounds. *Environmental Science & Technology*, *48*(11), 6309–6317. https://doi.org/10.1021/es500362a

Lee, J. Y., Daube, C., Fortner, E., Ellsworth, N., May, N. W., Tallant, J., et al. (2023). Chemical characterization of prescribed burn emissions from a mixed forest in Northern Michigan. *Environmental Sciences: Atmos.*, *3*(1), 35–48. https://doi.org/10.1039/D2EA00069E

Leskinen, A., Yli-Pirilä, P., Kuuspalo, K., Sippula, O., Jalava, P., Hirvonen, M.-R., et al. (2015). Characterization and testing of a new environmental chamber. *Atmospheric Measurement Techniques*, *8*(6), 2267–2278. https://doi.org/10.5194/amt-8-2267-2015

Li, Y., Pöschl, U., & Shiraiwa, M. (2016). Molecular corridors and parameterizations of volatility in the chemical evolution of organic aerosols. *Atmospheric Chemistry and Physics*, *16*(5), 3327–3344. https://doi.org/10.5194/acp-16-3327-2016

Lim, C. Y., Hagan, D. H., Coggon, M. M., Koss, A. R., Sekimoto, K., de Gouw, J., et al. (2019). Secondary organic aerosol formation from the laboratory oxidation of biomass burning emissions. *Atmospheric Chemistry and Physics*, *19*(19), 12797–12809. https://doi.org/10.5194/acp-19-12797-2019

Lindaas, J., Pollack, I. B., Calahorrano, J. J., O'Dell, K., Garofalo, L. A., Pothier, M. A., et al. (2021). Empirical insights into the fate of ammonia in western U.S. Wildfire smoke plumes. *Journal of Geophysical Research: Atmospheres*, *126*(11), e2020JD033730. https://doi.org/10.1029/2020JD033730

Liu, S., Aiken, A. C., Arata, C., Dubey, M. K., Stockwell, C. E., Yokelson, R. J., et al. (2014). Aerosol single scattering albedo dependence on biomass combustion efficiency: Laboratory and field studies. *Geophysical Research Letters*, *41*(2), 748. https://doi.org/10.1002/2013GL058392

Lopez-Hilfiker, F. D., Mohr, C., Ehn, M., Rubach, F., Kleist, E., Wildt, J., et al. (2014). A novel method for online analysis of gas and particle composition: Description and evaluation of a filter inlet for gases and AEROsols (FIGAERO). *Atmospheric Measurement Techniques*, *7*(4), 983–1001. https://doi.org/10.5194/amt-7-983-2014

Luo, J., Li, Z., Qiu, J., Zhang, Y., Fan, C., Li, L., et al. (2023). The simulated source apportionment of light absorbing aerosols: Effects of microphysical properties of partially-coated black carbon. *Journal of Geophysical Research: Atmospheres*, *128*(10), e2022JD037291. https://doi.org/10.1029/2022JD037291

May, A. A., Levin, E. J. T., Hennigan, C. J., Riipinen, I., Lee, T., Collett, J. L., Jr., et al. (2013). Gas-particle partitioning of primary organic aerosol emissions: 3. Biomass burning. *Journal of Geophysical Research: Atmospheres*, *118*(19), 11327–11338. https://doi.org/10.1002/jgrd.50828

May, A. A., McMeeking, G. R., Lee, T., Taylor, J. W., Craven, J. S., Burling, I., et al. (2014). Aerosol emissions from prescribed fires in the United States: A synthesis of laboratory and aircraft measurements. *Journal of Geophysical Research: Atmospheres*, *119*(20), 11826–11849. https://doi.org/10.1002/2014JD021848

McCarty, J. L., Aalto, J., Paunu, V.-V., Arnold, S. R., Eckhardt, S., Klimont, Z., et al. (2021). Reviews and syntheses: Arctic fire regimes and emissions in the 21st century. *Biogeosciences*, *18*(18), 5053–5083. https://doi.org/10.5194/bg-18-5053-2021

McClure, C. D., Lim, C. Y., Hagan, D. H., Kroll, J. H., & Cappa, C. D. (2020). Biomass-burning-derived particles from a wide variety of fuels–Part 1: Properties of primary particles. *Atmospheric Chemistry and Physics*, *20*(3), 1531–1547. https://doi.org/10.5194/acp-20-1531-2020

Milic, A., Mallet, M. D., Cravigan, L. T., Alroe, J., Ristovski, Z. D., Selleck, P., et al. (2017). Biomass burning and biogenic aerosols in northern Australia during the SAFIRED campaign. *Atmospheric Chemistry and Physics*, *17*(6), 3945–3961. https://doi.org/10.5194/acp-17-3945-2017

Müller, T., Laborde, M., Kassell, G., & Wiedensohler, A. (2011). Design and performance of a three-wavelength LED-based total scatter and backscatter integrating nephelometer. *Atmospheric Measurement Techniques*, *4*(6), 1291–1303. https://doi.org/10.5194/amt-4-1291-2011

Nault, B. A., Croteau, P., Jayne, J., Williams, A., Williams, L., Worsnop, D., et al. (2023). Laboratory evaluation of organic aerosol relative ionization efficiencies in the aerodyne aerosol mass spectrometer and aerosol chemical speciation monitor. *Aerosol Science and Technology*, *57*(10), 981–997. https://doi.org/10.1080/02786826.2023.2223249

Ng, N. L., Canagaratna, M. R., Zhang, Q., Jimenez, J. L., Tian, J., Ulbrich, I. M., et al. (2010). Organic aerosol components observed in Northern Hemispheric datasets from Aerosol Mass Spectrometry. *Atmospheric Chemistry and Physics*, *10*(10), 4625–4641. https://doi.org/10.5194/acp-10-4625-2010

Ng, N. L., Herndon, S. C., Trimborn, A., Canagaratna, M. R., Croteau, P. L., Onasch, T. B., et al. (2011). An aerosol chemical speciation monitor (ACSM) for routine monitoring of the composition and mass concentrations of ambient aerosol. *Aerosol Science and Technology*, *45*(7), 780–794. https://doi.org/10.1080/02786826.2011.560211

O'Dell, K., Ford, B., Fischer, E. V., & Pierce, J. R. (2019). Contribution of wildland-fire smoke to US PM2.5 and its influence on recent trends. *Environmental Science & Technology*, *53*(4), 1797–1804. https://doi.org/10.1021/acs.est.8b05430

Pagonis, D., Selimovic, V., Campuzano-Jost, P., Guo, H., Day, D. A., Schueneman, M. K., et al. (2023). Impact of biomass burning organic aerosol volatility on smoke concentrations downwind of fires. *Environmental Science & Technology*, *57*(44), 17011–17021. https://doi.org/10.1021/acs.est.3c05017

Permar, W., Wang, Q., Selimovic, V., Wielgasz, C., Yokelson, R. J., Hornbrook, R. S., et al. (2021). Emissions of trace organic gases from western U.S. Wildfires based on WE-CAN aircraft measurements. *Journal of Geophysical Research: Atmospheres*, *126*(11), e2020JD033838. https://doi.org/10.1029/2020JD033838

Pokhrel, R. P., Gordon, J., Fiddler, M. N., & Bililign, S. (2020). Impact of combustion conditions on physical and morphological properties of biomass burning aerosol. *Aerosol Science and Technology*, *55*(1), 80–91. https://doi.org/10.1080/02786826.2020.1822512

Rogers, B. M., Soja, A. J., Goulden, M. L., & Randerson, J. T. (2015). Influence of tree species on continental differences in boreal fires and climate feedbacks. *Nature Geoscience*, *8*(3), 228–234. https://doi.org/10.1038/ngeo2352

Saleh, R., Cheng, Z., & Atwi, K. (2018). The Brown–black continuum of light-absorbing combustion aerosols. *Environmental Science and Technology Letters*, *5*(8), 508–513. https://doi.org/10.1021/acs.estlett.8b00305

Schade, J., Passig, J., Irsig, R., Ehlert, S., Sklorz, M., Adam, T., et al. (2019). Spatially shaped laser pulses for the simultaneous detection of polycyclic aromatic hydrocarbons as well as positive and negative inorganic ions in single particle mass spectrometry. *Analytical Chemistry*, *91*(15), 10282–10288. https://doi.org/10.1021/acs.analchem.9b02477

Schneider, J., Weimer, S., Drewnick, F., Borrmann, S., Helas, G., Gwaze, P., et al. (2006). Mass spectrometric analysis and aerodynamic properties of various types of combustion-related aerosol particles. *Aerosols/Microparticles Special Issue*, *258*(1), 37–49. https://doi.org/10.1016/j.ijms.2006.07.008

Schwarz, J. P., Katich, J. M., Lee, S. L., Thomson, D. S., & Watts, L. A. (2022). "Invisible bias" in the single particle soot photometer due to trigger deadtime. *Aerosol Science and Technology*, *56*(7), 623–635. https://doi.org/10.1080/02786826.2022.2064265

Sekimoto, K., Koss, A. R., Gilman, J. B., Selimovic, V., Coggon, M. M., Zarzana, K. J., et al. (2018). High- and low-temperature pyrolysis profiles describe volatile organic compound emissions from western US wildfire fuels. *Atmospheric Chemistry and Physics*, *18*(13), 9263–9281. https://doi.org/10.5194/acp-18-9263-2018

Selimovic, V., Yokelson, R. J., Warneke, C., Roberts, J. M., de Gouw, J., Reardon, J., & Griffith, D. W. T. (2018). Aerosol optical properties and trace gas emissions by PAX and OP-FTIR for laboratory-simulated western US wildfires during FIREX. *Atmospheric Chemistry and Physics*, *18*(4), 2929–2948. https://doi.org/10.5194/acp-18-2929-2018

Shea, R. W., Shea, B. W., Kauffman, J. B., Ward, D. E., Haskins, C. I., & Scholes, M. C. (1996). Fuel biomass and combustion factors associated with fires in savanna ecosystems of South Africa and Zambia. *Journal of Geophysical Research*, *101*(D19), 23551–23568. https://doi.org/10.1029/95JD02047

Shorohova, E., Kneeshaw, D., Kuuluvainen, T., & Gauthier, S. (2011). Variability and dynamics of old-growth forests in the circumboreal zone: Implications for conservation, restoration and management. *Silva Fennica*, *45*(5), 785–806. https://doi.org/10.14214/sf.72

Sinha, A., George, I., Holder, A., Preston, W., Hays, M., & Grieshop, A. P. (2023). Development of volatility distributions for organic matter in biomass burning emissions. *Environmental Science: Atmospheres*, *3*(1), 11–23. https://doi.org/10.1039/D2EA00080F

Stier, P., Feichter, J., Kinne, S., Kloster, S., Vignati, E., Wilson, J., et al. (2005). The aerosol-climate model ECHAM5-HAM. *Atmospheric Chemistry and Physics*, *5*(4), 1125–1156. https://doi.org/10.5194/acp-5-1125-2005

Stockwell, C. E., Veres, P. R., Williams, J., & Yokelson, R. J. (2015). Characterization of biomass burning emissions from cooking fires, peat, crop residue, and other fuels with high-resolution proton-transfer-reaction time-of-flight mass spectrometry. *Atmospheric Chemistry and Physics*, *15*(2), 845–865. https://doi.org/10.5194/acp-15-845-2015

Stockwell, C. E., Yokelson, R. J., Kreidenweis, S. M., Robinson, A. L., DeMott, P. J., Sullivan, R. C., et al. (2014). Trace gas emissions from combustion of peat, crop residue, domestic biofuels, grasses, and other fuels: Configuration and fourier transform infrared (FTIR) component of the fourth fire Lab at missoula experiment (FLAME-4). *Atmospheric Chemistry and Physics*, *14*(18), 9727–9754. https://doi.org/10.5194/acp-14-9727-2014

Taylor, J. W., Wu, H., Szpek, K., Bower, K., Crawford, I., Flynn, M. J., et al. (2020). Absorption closure in highly aged biomass burning smoke. *Atmospheric Chemistry and Physics*, *20*(19), 11201–11221. https://doi.org/10.5194/acp-20-11201-2020

Tiitta, P., Leskinen, A., Hao, L., Yli-Pirilä, P., Kortelainen, M., Grigonyte, J., et al. (2016). Transformation of logwood combustion emissions in a smog chamber: Formation of secondary organic aerosol and changes in the primary organic aerosol upon daytime and nighttime aging. *Atmospheric Chemistry and Physics*, *16*(20), 13251–13269. https://doi.org/10.5194/acp-16-13251-2016

Vakkari, V., Beukes, J. P., Dal Maso, M., Aurela, M., Josipovic, M., & van Zyl, P. G. (2018). Major secondary aerosol formation in southern African open biomass burning plumes. *Nature Geoscience*, *11*(8), 580–583. https://doi.org/10.1038/s41561-018-0170-0

Vakkari, V., Kerminen, V.-M., Beukes, J. P., Tiitta, P., van Zyl, P. G., Josipovic, M., et al. (2014). Rapid changes in biomass burning aerosols by atmospheric oxidation. *Geophysical Research Letters*, *41*(7), 2644–2651. https://doi.org/10.1002/2014GL059396

Vakkari, V., Vettikat, L., Kommula, S., Mukherjee, A., Hao, L., Backman, J., et al. (2025). Data for laboratory experiments on savannah and European boreal forest fire emissions [Dataset]. *Finnish Meteorological Institute*. https://doi.org/10.57707/FMI-B2SHARE.16D432B62932448FBBF5CA38AAAEF603

van Wees, D., van der Werf, G. R., Randerson, J. T., Rogers, B. M., Chen, Y., Veraverbeke, S., et al. (2022). Global biomass burning fuel consumption and emissions at 500\,m spatial resolution based on the Global Fire Emissions Database (GFED). *Geoscientific Model Development*, *15*(22), 8411–8437. https://doi.org/10.5194/gmd-15-8411-2022

Vernooij, R., Eames, T., Russell-Smith, J., Yates, C., Beatty, R., Evans, J., et al. (2023). Dynamic savanna burning emission factors based on satellite data using a machine learning approach. *Earth System Dynamics*, *14*(5), 1039–1064. https://doi.org/10.5194/esd-14-1039-2023

Vernooij, R., Winiger, P., Wooster, M., Strydom, T., Poulain, L., Dusek, U., et al. (2022). A quadcopter unmanned aerial system (UAS)-based methodology for measuring biomass burning emission factors. *Atmospheric Measurement Techniques*, *15*(14), 4271–4294. https://doi.org/10.5194/amt-15-4271-2022

Virkkula, A. (2021). Modeled source apportionment of black carbon particles coated with a light-scattering shell. *Atmospheric Measurement Techniques*, *14*(5), 3707–3719. https://doi.org/10.5194/amt-14-3707-2021

Virkkula, A., Pohja, T., Aalto, P. P., Keronen, P., Schobesberger, S., Clements, C. B., et al. (2014). Airborne measurements of aerosols and carbon dioxide during a prescribed fire experiment at a boreal forest site. *Boreal Environment Research*, *19*, 153–181.

Ward, D. E., & Radke, L. F. (1993). Emissions measurements from vegetation fires: A comparative evaluation of methods and results. In P. J. Crutzen & J. G. Goldammer (Eds.), *Fire in the environment: The ecological, atmospheric and climatic importance of vegetation fires* (pp. 53–76). John Wiley.

Warneke, C., Schwarz, J. P., Dibb, J., Kalashnikova, O., Frost, G., Al-Saad, J., et al. (2023). Fire influence on regional to global environments and air quality (FIREX-AQ). *Journal of Geophysical Research: Atmospheres*, *128*(2), e2022JD037758. https://doi.org/10.1029/2022JD037758

Wu, H., Taylor, J. W., Langridge, J. M., Yu, C., Allan, J. D., Szpek, K., et al. (2021). Rapid transformation of ambient absorbing aerosols from West African biomass burning. *Atmospheric Chemistry and Physics*, *21*(12), 9417–9440. https://doi.org/10.5194/acp-21-9417-2021

Wu, H., Taylor, J. W., Szpek, K., Langridge, J. M., Williams, P. I., Flynn, M., et al. (2020). Vertical variability of the properties of highly aged biomass burning aerosol transported over the southeast Atlantic during CLARIFY-2017. *Atmospheric Chemistry and Physics*, *20*(21), 12697–12719. https://doi.org/10.5194/acp-20-12697-2020

Xu, W., Lambe, A., Silva, P., Hu, W., Onasch, T., Williams, L., et al. (2018). Laboratory evaluation of species-dependent relative ionization efficiencies in the Aerodyne Aerosol Mass Spectrometer. *Aerosol Science and Technology*, *52*(6), 626–641. https://doi.org/10.1080/02786826.2018.1439570

Ylisirniö, A., Barreira, L. M. F., Pullinen, I., Buchholz, A., Jayne, J., Krechmer, J. E., et al. (2021). On the calibration of FIGAERO-ToF-CIMS: Importance and impact of calibrant delivery for the particle-phase calibration. *Atmospheric Measurement Techniques*, *14*(1), 355–367. https://doi.org/10.5194/amt-14-355-2021

Yokelson, R. J., Bertschi, I. T., Christian, T. J., Hobbs, P. V., Ward, D. E., & Hao, W. M. (2003). Trace gas measurements in nascent, aged, and cloud-processed smoke from African savanna fires by airborne Fourier transform infrared spectroscopy (AFTIR). *Journal of Geophysical Research*, *108*(D13), 8478. https://doi.org/10.1029/2002JD002322

Yokelson, R. J., Burling, I. R., Urbanski, S. P., Atlas, E. L., Adachi, K., Buseck, P. R., et al. (2011). Trace gas and particle emissions from open biomass burning in Mexico. *Atmospheric Chemistry and Physics*, *11*(14), 6787–6808. https://doi.org/10.5194/acp-11-6787-2011

Yokelson, R. J., Goode, J. G., Ward, D. E., Susott, R. A., Babbitt, R. E., Wade, D. D., et al. (1999). Emissions of formaldehyde, acetic acid, methanol, and other trace gases from biomass fires in North Carolina measured by airborne Fourier transform infrared spectroscopy. *Journal of Geophysical Research*, *104*(D23), 30109–30125. https://doi.org/10.1029/1999JD900817

Zanatta, M., Gysel, M., Bukowiecki, N., Müller, T., Weingartner, E., Areskoug, H., et al. (2016). A European aerosol phenomenology-5: Climatology of black carbon optical properties at 9 regional background sites across Europe. *Atmospheric Environment*, *145*, 346–364. https://doi.org/10.1016/j.atmosenv.2016.09.035

Zotter, P., Herich, H., Gysel, M., El-Haddad, I., Zhang, Y., Močnik, G., et al. (2017). Evaluation of the absorption Ångström exponents for traffic and wood burning in the Aethalometer-based source apportionment using radiocarbon measurements of ambient aerosol. *Atmospheric Chemistry and Physics*, *17*(6), 4229–4249. https://doi.org/10.5194/acp-17-4229-2017